Nonlinearity **12** (1999) 103–140. Printed in the UK PII: S0951-7715(99)95148-4

Dynamics of the parametrically driven NLS solitons beyond the onset of the oscillatory instability

N V Alexeeva†, I V Barashenkov‡ and D E Pelinovsky§

Department of Applied Mathematics, University of Cape Town, Private Bag Rondebosch 7701, South Africa

Received 15 June 1998, in final form 3 November 1998
Recommended by E B Bogomolny

Abstract. Solitary waves in conservative and near-conservative systems may become unstable due to a resonance of two internal oscillation modes. We study the parametrically driven, damped nonlinear Schrödinger equation, a prototype system exhibiting this oscillatory instability. An asymptotic multi-scale expansion is used to derive a reduced amplitude equation describing the nonlinear stage of the instability and supercritical dynamics of the soliton in the *weakly* dissipative case. We also derive the amplitude equation in the *strongly* dissipative case, when the bifurcation is of the Hopf type. The analysis of the reduced equations shows that in the *undamped* case the temporally periodic spatially localized structures are suppressed by the nonlinearity-induced radiation. In this case the unstable stationary soliton evolves either into a slowly decaying long-lived breather, or into a radiating soliton whose amplitude grows without bound. However, adding a small damping is sufficient to bring about a stably oscillating soliton of finite amplitude.

PACS numbers: 0340K, 0545, 7530D

1. Introduction and motivation

Soliton solutions are known to be of paramount importance for nonlinear dispersive systems. Stable solitons dominate the long-term asymptotic behaviour of spatially inhomogeneous initial conditions. Unstable solitons can nucleate collapses [1], spatially localized temporally periodic and chaotic states [2, 3], spatio-temporal chaos [4] and phase transitions [5]. The nonlinear evolution of a linearly unstable soliton can often be predicted from knowing the *mechanism* of its instability. Until the early 1990s, the onset of soliton instability in conservative systems was typically associated with the transition of a linearized eigenvalue from the imaginary to positive real axis (see e.g. [6, 7] and references therein). In the case of the nonlinear Schrödinger (NLS) equations that we will be concerned with in this paper, the nonlinear evolution of this instability (usually referred to as the *translational* instability) may follow a limited number of scenarios: unstable *bright* solitons blow up, disperse away, or evolve into a long-lived oscillating structure asymptotically settling to a stable stationary soliton [8]; unstable *dark* solitons dissociate into a couple or inflate [5, 9].

† Current address: Department of Physics, University of Crete, PO Box 2208, 71003 Heraklion, Crete, Greece. E-mail addresses: nora@maths.uct.ac.za, nora@ianos.physics.uch.gr
‡ Current address: Department of Physics, University of Crete, PO Box 2208, 71003 Heraklion, Crete, Greece. E-mail addresses: igor@maths.uct.ac.za, igor@physics.uch.gr
§ Current address: Department of Mathematics, University of Toronto, 100 St George Street, Toronto, Ontario, Canada M5S 3G3. E-mail address: dmpeli@math.toronto.edu

0951-7715/99/010103+38$19.50

More recently it was realized that there are also different mechanisms of soliton instability; in particular, the soliton can be destroyed as a result of a resonance of two internal oscillation modes [10–12]. The objective of this paper is to follow the nonlinear development of this new instability (known as the *oscillatory* instability) and describe supercritical dynamical regimes of solitons. As a prototype nonlinear PDE, we adopt the parametrically driven, damped NLS equation:

$$\mathrm{i}\psi_T + \psi_{XX} - \psi + 2|\psi|^2\psi = \mathfrak{h}\psi^* - \mathrm{i}\gamma\psi. \tag{1}$$

Here $\mathfrak{h}$ is the amplitude of the driver and γ the dissipation coefficient; the frequency of the driver has been normalized to unity. This equation describes a variety of physical phenomena, including the nonlinear Faraday resonance in water [3, 13, 14]; parametric instabilities of waves in plasma [15]; the parametric generation of spin waves and magnetic solitons in ferromagnets and antiferromagnets [11, 16, 17] and, finally, the effect of phase-sensitive parametric amplifiers on solitons propagating in optical fibres [18]. It also serves as an amplitude equation for small-amplitude, parametrically driven sine-Gordon breathers [11] and hence its range of applicability includes all systems modelled by the parametrically driven sine-Gordon equation [19].

When the driver's amplitude is very large, $\mathfrak{h}^2 > 1 + \gamma^2$, the trivial solution $\psi = 0$ of equation (1) is unstable against continuous spectrum perturbations [11]. (This is what physicists call 'parametric instability' [3, 13–17].) In this paper we will be concerned with a complementary region, $\mathfrak{h}^2 < 1 + \gamma^2$, and so the trivial solution will always be deemed stable. In this region equation (1) has two stationary soliton solutions. One of these is always unstable and will be disregarded in the bulk of this paper. The other one is stable for small driving strengths but loses its stability as $\mathfrak{h}$ is increased for the fixed dissipation coefficient. In the undamped case ($\gamma = 0$) the instability arises due to the collision of two pure imaginary eigenvalues of the associated linearized operator, one detaching from the continuous spectrum and the other one originating from the broken $U(1)$ gauge invariance [11]. The two imaginary eigenvalues collide at a critical value $\mathfrak{h} = \mathfrak{h}_c \approx 0.064$ and then emerge into the complex plane producing the oscillatory instability (and hence the oscillatory-instability bifurcation) of the soliton. The linearized stability problem for the full, dissipative case can be reduced, by a nonlinear eigenvalue transformation [11], to the one for the undamped equation. Roughly speaking, this transformation subtracts γ from all eigenvalues so that the instability occurs for larger values of $\mathfrak{h}$, when a pair of complex-conjugate eigenvalues crosses the line $\mathrm{Re}\,\lambda = 0$. This is now a Hopf bifurcation, typical of dissipative systems.

A natural question is what localized nonlinear structures serve as attractors in the supercritical domain (i.e. beyond the onset of the oscillatory and Hopf bifurcations, respectively). In the dissipative case ($\gamma \neq 0$) this was addressed by means of direct computer simulations of equation (1) [4]. It was observed that in the neighbourhood of the transition curve on the $(\gamma, \mathfrak{h})$-plane, the stationary soliton is replaced by a temporally periodic one. Having fixed some γ in the range $0 < \gamma < 0.37$ and increasing $\mathfrak{h}$, the soliton undergoes the period-doubling (for γ smaller than 0.25) or quasiperiodic (for $0.25 \leqslant \gamma \leqslant 0.37$) transition to chaos [4]. (For $\gamma > 0.37$ the static soliton is stable in its entire domain of existence.)

In this paper we attempt to describe the supercritical dynamics of the soliton analytically. Our analysis is based on the reduced amplitude equations for the soliton's perturbation which we derive for $\mathfrak{h}$ in the neighbourhood of the oscillatory and the Hopf bifurcation. We also perform computer simulations of equation (1) in the Hamiltonian case ($\gamma = 0$) which has not been previously studied numerically. Results of these simulations are compared with conclusions of the finite-dimensional analysis. Although the $\gamma = 0$ case is clearly nongeneric (in the sense that some small damping is present in all underlying physical settings), it provides

insight into, and serves as a starting point for the analysis of the general, dissipative equation.

The plan and a brief summary of the paper is as follows. First in section 2, we consider the *weakly* dissipative regime, $\gamma \ll 1$, and derive a reduced amplitude equation describing the nonlinear evolution of the perturbation to the soliton in the vicinity of the bifurcation point ($\mathfrak{h} \sim \mathfrak{h}_c$). This amplitude equation is a complex nonlinear ODE of the second order. In the *strongly* dissipative regime, i.e. for $\gamma \sim 1$, the above second-order equation is replaced by the (first-order) complex Landau equation. The latter is derived in section 3. In some parts of our derivation we have to rely upon numerical solutions of eigenvalue and boundary value problems; details of the corresponding numerical algorithms have been relegated to the appendix. The subsequent section, section 4, contains a detailed analysis of solutions to the above finite-dimensional system for the vanishing, small and finite γ. The upshot of this study is that no periodic solutions are possible in the $\gamma = 0$ case; all finite-dimensional trajectories escape to infinity. However, adding a small damping gives rise to a stable periodic orbit coexisting with unbounded motions. Finally, only periodic finite-dimensional trajectories survive when γ is made finite. In section 5 the conclusions based on the reduced amplitude equation for the undamped case are compared with results of numerical simulations of the full, nonreduced NLS equation (1). Consistently with the finite-dimensional predictions, no stably oscillating solitons were observed in these simulations. All localized initial conditions were seen to evolve either into a radiating soliton with the amplitude growing without bound, or into a slowly-decaying, small-amplitude breather-like solution (or possibly into a couple of diverging breathers.) The last section (section 6) contains concluding remarks and outlines some open problems.

2. Reduced amplitude equations for the oscillatory-instability bifurcation

2.1. Soliton solutions and linear corrections

The two stationary soliton solutions of the parametrically driven, damped NLS equation (1) are given by [11, 14]:

$$\psi_\pm = A_\pm \mathrm{e}^{-\mathrm{i}\theta_\pm} \operatorname{sech}(A_\pm X), \tag{2a}$$

where

$$\sin 2\theta_\pm = \frac{\gamma}{\mathfrak{h}}, \qquad \cos 2\theta_\pm = \pm\sqrt{1 - \frac{\gamma^2}{\mathfrak{h}^2}} \tag{2b}$$

and

$$A_\pm^2 = 1 \pm \sqrt{\mathfrak{h}^2 - \gamma^2}. \tag{2c}$$

The two solitons emerge via a saddle-node bifurcation at $\mathfrak{h} = \gamma$. The ψ_+ soliton is stable in some neighbourhood of the bifurcation point while the ψ_- always has a positive linearized eigenvalue and hence is unstable for *all* $\mathfrak{h}$ and γ. Since this unstable soliton does not undergo any further bifurcations, we are disregarding it and concentrating on the ψ_+ in what follows. (We will only return to the evolution of the instability of the ψ_- soliton when we present results of our numerical simulations in section 5.)

Since we are interested in solutions which are close to the soliton (2) in some sense, it is convenient to rescale variables as

$$X = \frac{x}{A}, \qquad T = \frac{t}{A^2}$$

and decompose ψ into its real and imaginary part as

$$\psi = A\{U(x,t) + \mathrm{i}V(x,t)\}\mathrm{e}^{-\mathrm{i}\theta}. \tag{3}$$

Here $A = A_+$ and $\theta = \theta_+$; the subscript was omitted. Defining

$$H = \frac{(\mathfrak{h}^2 - \gamma^2)^{1/2}}{A^2}, \qquad \Gamma = \frac{\gamma}{A^2},$$

the equation (1) becomes

$$-V_t - 2\Gamma V = -U_{xx} + U - 2(U^2 + V^2)U, \tag{4a}$$

$$U_t + 2HV = -V_{xx} + V - 2(U^2 + V^2)V. \tag{4b}$$

The soliton solution of equation (4) is now

$$U_0 = \operatorname{sech} x, \qquad V_0 = 0.$$

Linearizing equation (4) about the soliton,

$$U = U_0(x) + \varepsilon f(x)\mathrm{e}^{\mathrm{i}\Omega t}, \qquad V = \mathrm{i}\varepsilon g(x)\mathrm{e}^{\mathrm{i}\Omega t}, \tag{5}$$

where ε is a small parameter, gives an eigenvalue problem for f and g:

$$\begin{pmatrix} L_1 & 2\mathrm{i}\Gamma \\ 0 & L_2 \end{pmatrix} \begin{pmatrix} f \\ g \end{pmatrix} = \Omega \begin{pmatrix} 0 & 1 \\ 1 & 0 \end{pmatrix} \begin{pmatrix} f \\ g \end{pmatrix}. \tag{6}$$

Here

$$L_1 = -\frac{\partial^2}{\partial x^2} + 1 - 6\operatorname{sech}^2 x, \tag{7}$$

$$L_2 = -\frac{\partial^2}{\partial x^2} + 1 - 2H - 2\operatorname{sech}^2 x, \tag{8}$$

and the eigenvalue Ω is the frequency of the perturbed soliton's oscillations. In studies of stability problems it is more common to deal with the quantity $\lambda = \mathrm{i}\Omega$ which is referred to as the 'linearized eigenvalue', or 'stability eigenvalue'. However, the frequency Ω turns out to be more suitable for our present purposes. Occasionally we will make reference to λ as well.

The damped eigenvalue problem (6) can be reduced, via a nonlinear eigenvalue transformation [11], to the one with $\Gamma = 0$:

$$\begin{pmatrix} L_1 & 0 \\ 0 & L_2 \end{pmatrix} \begin{pmatrix} u \\ v \end{pmatrix} = \omega \begin{pmatrix} 0 & 1 \\ 1 & 0 \end{pmatrix} \begin{pmatrix} u \\ v \end{pmatrix}, \tag{9a}$$

or equivalently,

$$\Lambda \begin{pmatrix} u \\ v \end{pmatrix} \equiv \begin{pmatrix} 0 & L_2 \\ L_1 & 0 \end{pmatrix} \begin{pmatrix} u \\ v \end{pmatrix} = \omega \begin{pmatrix} u \\ v \end{pmatrix}. \tag{9b}$$

Here

$$\omega = z\Omega, \qquad z = \left(1 - \frac{2\mathrm{i}\Gamma}{\Omega}\right)^{1/2}, \tag{10a}$$

and

$$u = f, \qquad v = zg. \tag{10b}$$

As it was shown, numerically, in [11], the operator Λ has two pairs of nonzero discrete eigenvalues, $\pm\omega_a$ and $\pm\omega_b$. For $H < H_c$, these eigenvalues are real and lie in the gap of the continuous spectrum: $\omega_a, \omega_b < \sqrt{1 - 2H}$ (see figure 1). As H reaches the critical value $H_c \approx 0.060$, the two eigenvalues merge ($\omega_a, \omega_b \to \omega_c \approx 0.83$), and then immediately split up moving into the complex plane (figure 1). In the undamped case ($\Gamma = 0$), this implies the oscillatory bifurcation. For $H > H_c$ the solution is unstable; the nonlinear evolution of this oscillatory instability will result in some other nonlinear attractors. In the next two subsections

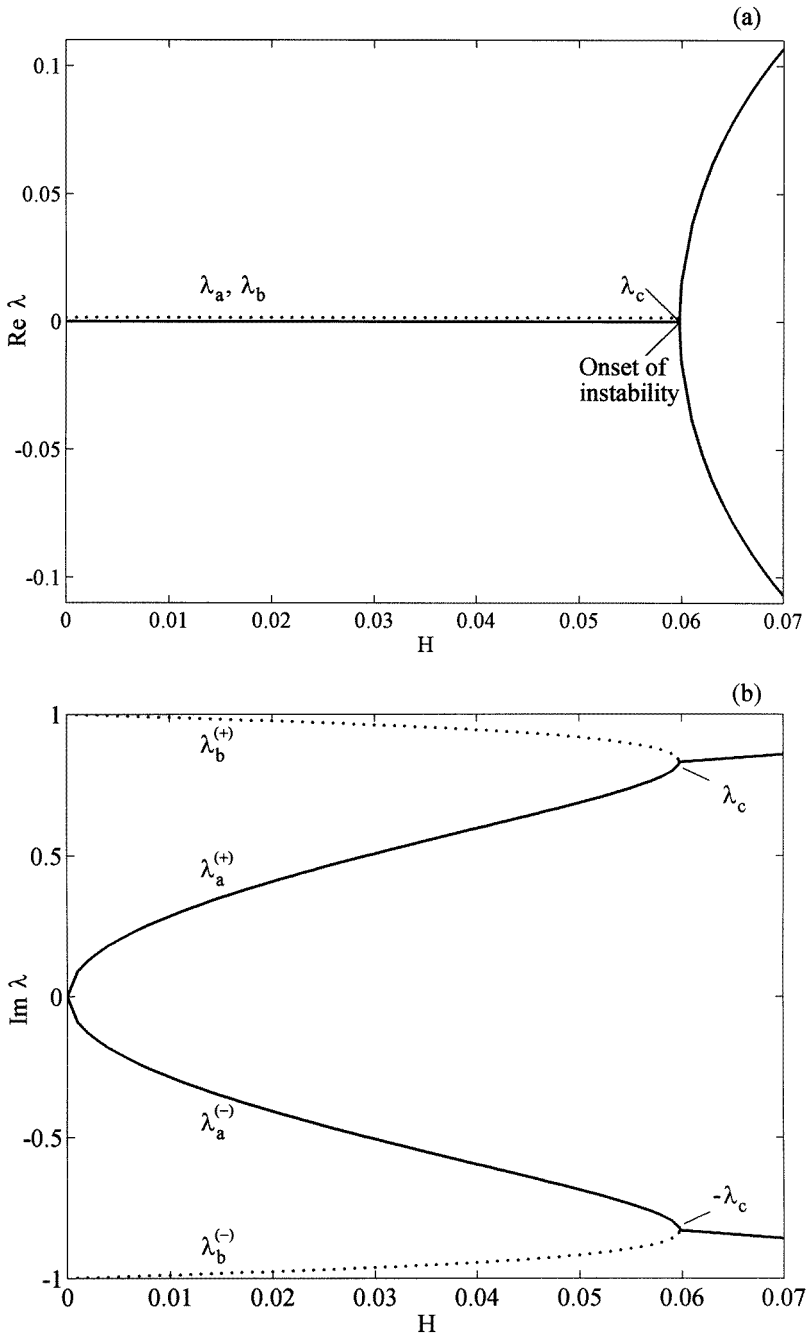

Figure 1. The bifurcation diagram for $\gamma = 0$. Real (*a*) and imaginary (*b*) parts of the eigenvalues $\lambda = \mathrm{i}\omega$ are shown as functions of H. The complex plane in (*c*) results from the combination of (*a*) and (*b*). The wavy line on (*c*) depicts the continuous spectrum and the dotted lines show the imaginary eigenvalues $\lambda_b^{(\pm)} = \pm\mathrm{i}\omega_b$ detaching from the continuum. The oscillatory instability sets in when two pairs of imaginary eigenvalues merge at $H = H_c$ ($i\omega_a, \mathrm{i}\omega_b \to \mathrm{i}\omega_c$) and become a complex quadruplet.

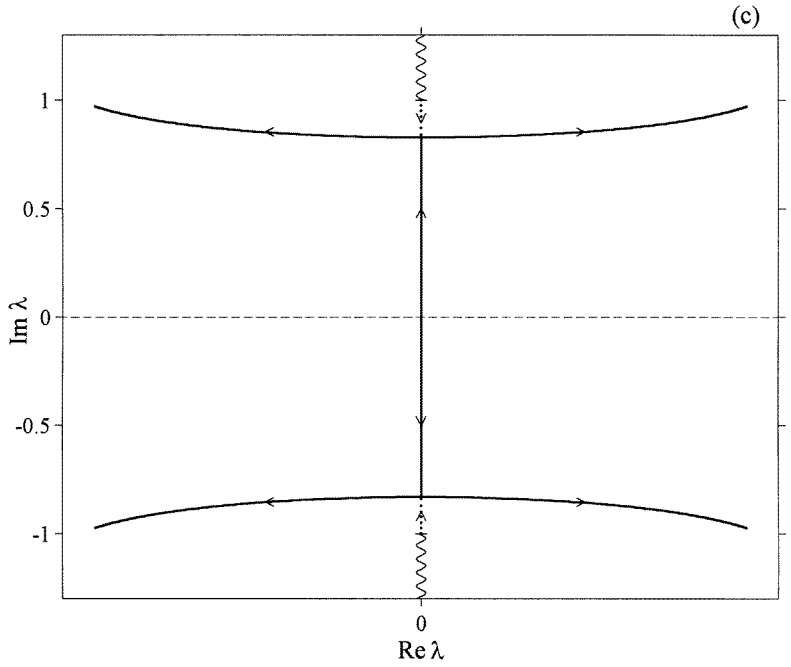

Figure 1. (Continued)

we develop an asymptotic formalism which captures the essentials of the nonlinear dynamics of the unstable soliton in this supercritical domain.

In the weakly dissipative case (Γ small but nonzero) the instability sets in not at $H = H_c$ but later, when the real part of $\lambda = \mathrm{i}\Omega$ becomes positive (see figures 2(*a*) and (*c*)). In literature, this would be usually referred to as the *Hopf* bifurcation. However, the asymptotic formalism associated with the *oscillatory-instability* bifurcation provides an adequate description of supercritical dynamics in the weakly dissipative limit as well. More importantly, the resulting amplitude equation is fundamentally different from the normal form of the Hopf bifurcation (see below). For this reason we will be using the term 'oscillatory-instability bifurcation' not only when $\Gamma = 0$ but also in the small-Γ case.

2.2. Asymptotic analysis: second-order corrections

Now we are prepared to derive a reduced nonlinear model describing the evolution of the perturbations to the stationary soliton (5) in the vicinity of the bifurcation value $H = H_c$ in the nearly conservative case, $\Gamma \sim 0$. The derivation is facilitated by factorizing the complex amplitude of the linear part of the perturbation (assumed small) as ϵa. Here $a = \mathrm{O}(1)$ and ϵ is a dimensionless small parameter; the perturbation is also assumed to be slowly varied: $a = a(\tau)$, where $\tau = \epsilon t$. We expand U and V in the asymptotic series in ϵ:

$$U = U_0(x) + \sum_{n=1}^{\infty} \epsilon^n U_n(x, t, \tau), \tag{11a}$$

$$V = \sum_{n=1}^{\infty} \epsilon^n V_n(x, t, \tau), \tag{11b}$$

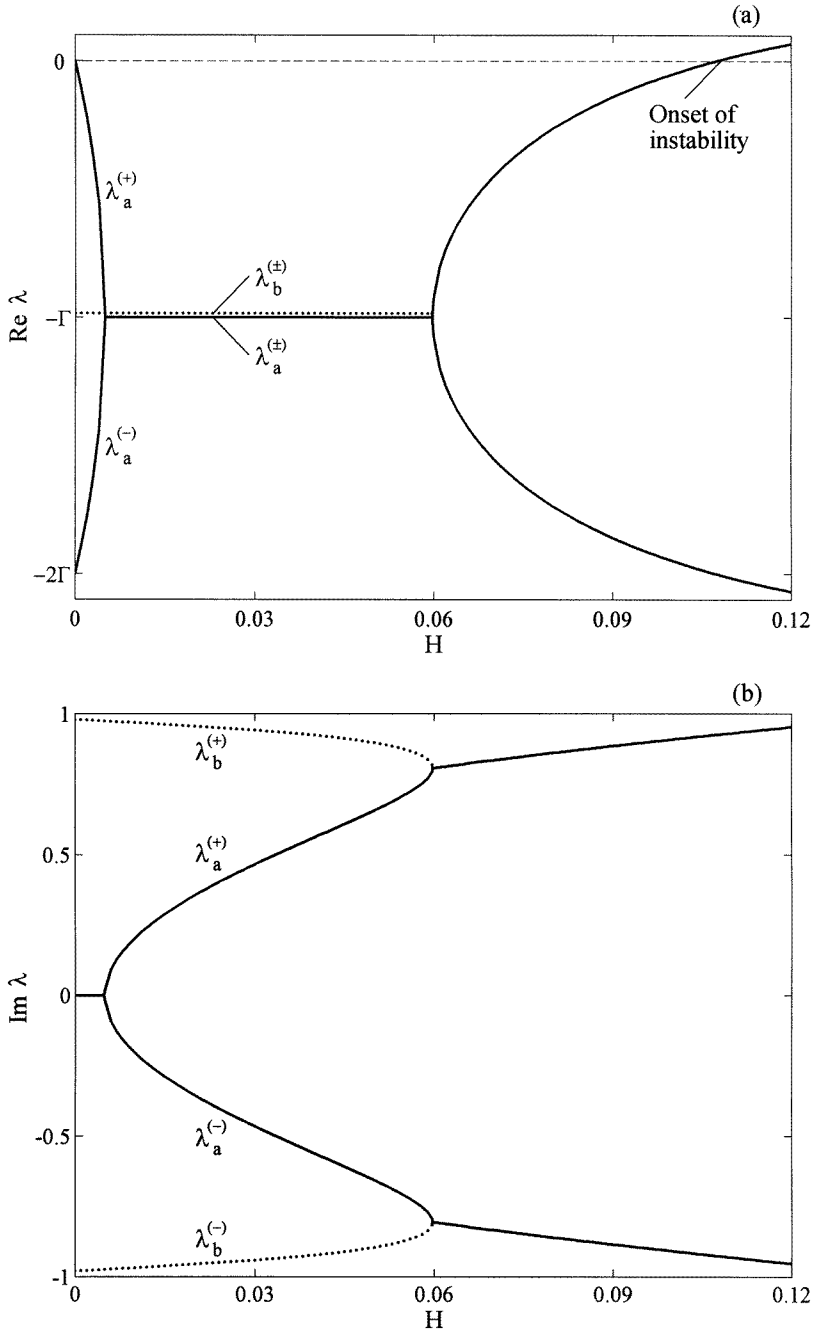

Figure 2. The bifurcation diagram for $\gamma \neq 0$. (In this plot $\Gamma = 0.2$). This diagram was obtained from the one in figure 1 by applying the transformation (10): $\lambda = -\Gamma \pm i(\omega^2 - \Gamma^2)^{1/2}$. For small H such that $\omega_a < \Gamma$, there is a pair of real eigenvalues $\lambda_a^{(\pm)} = -\Gamma \pm (\Gamma^2 - \omega_a^2)^{1/2}$ (full line). When ω_a exceeds Γ, an imaginary part appears while the real part remains fixed: $\lambda_a^{(\pm)} = -\Gamma \pm i(\omega_a^2 - \Gamma^2)^{1/2}$. Another pair of complex-conjugate eigenvalues is $\lambda_b^{(\pm)} = -\Gamma \pm i(\omega_b^2 - \Gamma^2)^{1/2}$ (dotted curve). At $H = H_c$, where $\omega_a = \omega_b$, the λ_a and λ_b eigenvalues merge pairwise, and the real parts start to grow. The instability sets in when Re λ crosses the horizontal zero line (broken) in (*a*).

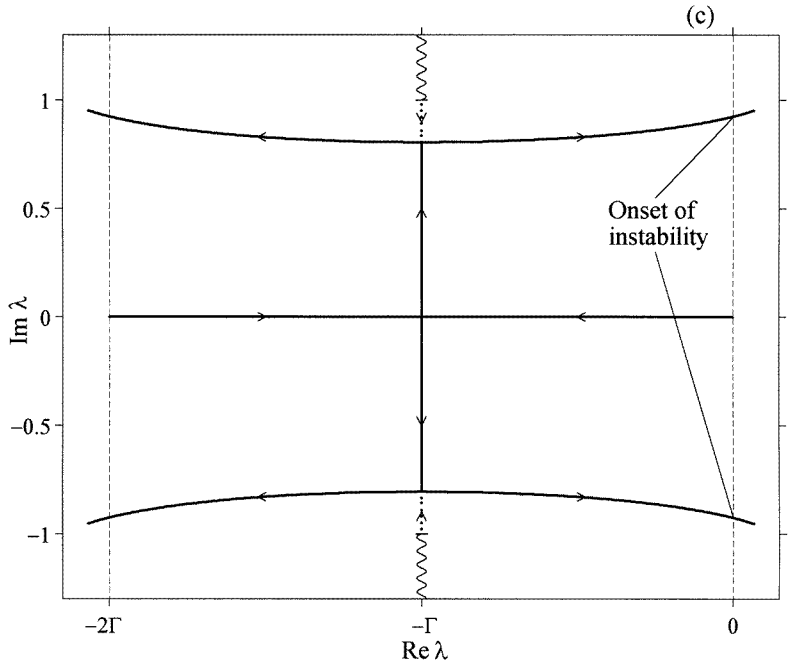

Figure 2. (Continued)

where $U_0 = \operatorname{sech} x$,

$$U_1 = [a(\tau)e^{i\omega_c t} + a^*(\tau)e^{-i\omega_c t}]u_c(x), \tag{12a}$$

$$V_1 = i[a(\tau)e^{i\omega_c t} - a^*(\tau)e^{-i\omega_c t}]v_c(x), \tag{12b}$$

and u_c, v_c are components of the eigenvector of the operator (9) associated with the eigenvalue $\omega = \omega_c$ and parameter value $H = H_c$. These functions are real-valued and exponentially decaying at infinities; we also assume that they are normalized to unity:

$$\int_{-\infty}^{\infty} (u_c^2 + v_c^2)\,dx = 1. \tag{13}$$

Writing

$$H = H_c + \epsilon^2 h, \qquad \Gamma = \epsilon\rho, \tag{14}$$

we include weak dissipative effects and a small deviation from the bifurcation point into the leading order of the asymptotic analysis. Substituting equations (11), (12) and (14) into the system (4), and equating coefficients of like powers of ϵ and equal harmonics, we obtain for the ϵ^2-correction:

$$U_2 = |a|^2 u_0(x) + 2\,\mathrm{Re}\left\{i\frac{da}{d\tau}e^{i\omega_c t}\right\} u_1(x) + 2\rho\,\mathrm{Re}\{iae^{i\omega_c t}\}u_\gamma(x) + 2\,\mathrm{Re}\{a^2 e^{2i\omega_c t}u_2(x)\}, \tag{15a}$$

$$V_2 = -2\,\mathrm{Re}\left\{\frac{da}{d\tau}e^{i\omega_c t}\right\} v_1(x) - 2\rho\,\mathrm{Re}\{ae^{i\omega_c t}\}v_\gamma(x) + 2\,\mathrm{Re}\{ia^2 e^{2i\omega_c t}v_2(x)\}, \tag{15b}$$

where the functions u_0, u_1, u_γ, u_2 and v_0, v_1, v_γ, v_2 are to be found by solving the following set of linear nonhomogeneous equations:

$$L_1 u_0 = 4U_0(3u_c^2 + v_c^2); \tag{16}$$

$$M_{\omega_c}\begin{pmatrix} u_1 \\ v_1 \end{pmatrix} \equiv \begin{pmatrix} L_1 & -\omega_c \\ -\omega_c & L_2 \end{pmatrix}\begin{pmatrix} u_1 \\ v_1 \end{pmatrix} = -\begin{pmatrix} v_c \\ u_c \end{pmatrix}; \tag{17}$$

$$M_{\omega_c}\begin{pmatrix} u_\gamma \\ v_\gamma \end{pmatrix} = -2\begin{pmatrix} v_c \\ 0 \end{pmatrix}; \tag{18}$$

$$M_{2\omega_c}\begin{pmatrix} u_2 \\ v_2 \end{pmatrix} \equiv \begin{pmatrix} L_1 & -2\omega_c \\ -2\omega_c & L_2 \end{pmatrix}\begin{pmatrix} u_2 \\ v_2 \end{pmatrix} = 2U_0\begin{pmatrix} 3u_c^2 - v_c^2 \\ 2u_c v_c \end{pmatrix}. \tag{19}$$

(Here the operator L_2 is defined by equation (7) with $H = H_c$.)

It is worthwhile to comment on the meaning of each term in equation (15) and the solvability of equations (16)–(19). First of all, the functions u_0, u_2, and v_2 represent the nonlinearity-induced corrections to the soliton's shape (zeroth and second harmonic, respectively.) The equation (16) always admits a solution decaying as $x \to \pm\infty$, since the corresponding homogeneous solution (the translational zero-frequency mode $f_T(x) = \tanh x \operatorname{sech} x$) is an odd function and therefore, is orthogonal to the even function on the right-hand side. On the contrary, the nonhomogeneous solution of equation (19) is bounded but does not have to decay at the infinities as there is no reason why the corresponding *homogeneous* solution should be orthogonal to the vector function on the right-hand side of (19). The homogeneous solution is the eigenfunction of the eigenvalue problem (9) associated with the eigenvalue $\omega = 2\omega_c \approx 1.66$. This eigenvalue belongs to the continuous spectrum and so the nonhomogeneous solution u_2, v_2 is defined up to the addition of an arbitrary combination of two continuous spectrum eigenfunctions†. Physically, the terms proportional to u_2 and v_2 are interpreted as the radiation emitted by the oscillating soliton. The boundary conditions corresponding to the *outgoing* radiation waves read

$$\begin{pmatrix} u_2 \\ v_2 \end{pmatrix} \to \begin{pmatrix} 1 \\ \frac{k_c^2+1}{2\omega_c} \end{pmatrix}\mathcal{R}^{\pm}\mathrm{e}^{\mp \mathrm{i}k_c x} \qquad \text{as} \quad x \to \pm\infty, \tag{20}$$

where the wavenumber k_c is positive, with

$$k_c^2 = \sqrt{H_c^2 + 4\omega_c^2} + H_c - 1. \tag{21}$$

With the above choice, the radiation terms in equation (15) reduce, as $x \to \pm\infty$, to the outgoing harmonic waves proportional to $\exp\{\mathrm{i}(2\omega_c t \mp k_c x)\}$. The functions u_2 and v_2 are, therefore, complex-valued. The functions on the right-hand side of equation (19) are even; it is not difficult to realize that this fact, together with the radiation conditions (20), requires that $u_2(x)$ and $v_2(x)$ should also be even. Hence, $\mathcal{R}^+ = \mathcal{R}^- \equiv \mathcal{R}$.

Before commenting on equations (17) and (18), we need to recall that ω_c is a *repeated* (double) eigenvalue of the operator (9) arising from the coalescence of two simple eigenvalues, ω_a and ω_b. The associated eigenvectors, $\{u_a, v_a\}$ and $\{u_b, v_b\}$, are orthogonal in the sense of the following ($SO(1,1)$-invariant) scalar product: $\int_{-\infty}^{\infty}(u_a v_b + u_b v_a)\,\mathrm{d}x = 0$. When ω_a and ω_b coalesce, the associated eigenvectors can either stay linearly independent (i.e. the double eigenvalue ω_c is complete) or collapse into one (i.e. ω_c is defective). Our numerical analysis shows that the second possibility occurs in the case at hand: when $H \to H_c$, we have $u_a, u_b \to u_c$ and $v_a, v_b \to v_c$. Consequently, the orthogonality condition at the point $H = H_c$ becomes

$$I_c \equiv 2\int_{-\infty}^{\infty} u_c v_c\,\mathrm{d}x = 0. \tag{22}$$

In order to illustrate the validity of equation (22), we have plotted the quadratic forms

$$I[u, v] = 2\int_{-\infty}^{\infty} uv\,\mathrm{d}x \tag{23}$$

† Here we use the term 'eigenfunction' simply for the sake of brevity; the continuous spectrum 'eigenfunctions' are, of course, non-normalizable.

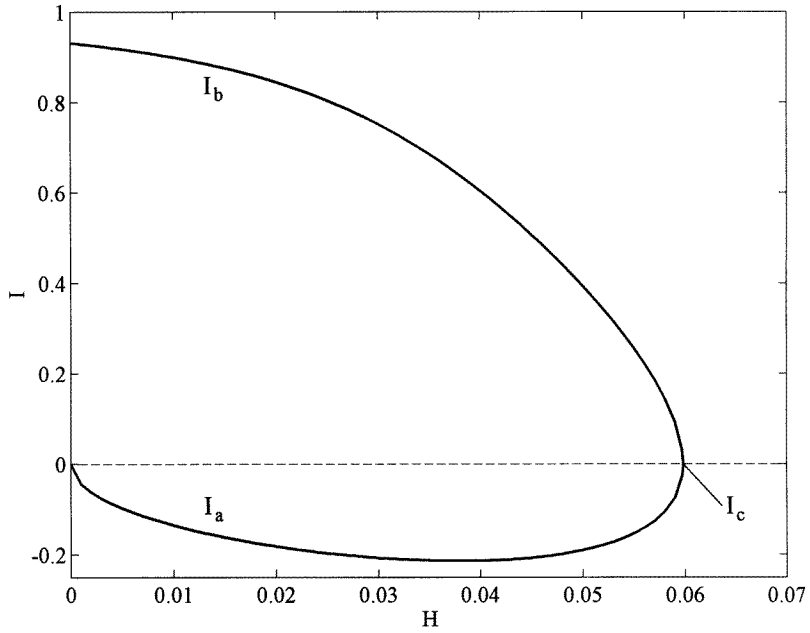

Figure 3. The quadratic form $I = 2\int uv\,\mathrm{d}x$, evaluated numerically for two soliton's internal modes, $\{u_a, v_a\}$ and $\{u_b, v_b\}$. When ω_a merges with ω_b, both I_a and I_b vanish ensuring the existence of the generalized eigenvector $\{u_1, v_1\}$ at the point $H = H_c$.

for the two eigenvectors of the linearized operator (9) (figure 3). The forms I_a and I_b are indeed seen to merge and vanish at $H = H_c$.

Turning to equation (17), we can now identify its solution $\{u_1, v_1\}$ as a rank-2 generalized eigenvector associated with the eigenvalue ω_c of the linearized operator (9). The solvability condition for equation (17) is nothing but the orthogonality relation (22); the fact that the quadratic form I_c of the eigenvector $\{u_c, v_c\}$ vanishes, guarantees that the generalized eigenvector $\{u_1, v_1\}$ exists and decays as $|x| \to \infty$. The real functions $u_1(x)$ and $v_1(x)$ can be interpreted as resonant ϵ^2-corrections to the linearised perturbation.

Finally, the same equation (22) gives the solvability condition for the system (18). The real functions u_γ and v_γ account for the ϵ^2-corrections due to the weak damping.

2.3. The reduced finite-dimensional system

Having found the second-order corrections, we proceed to the third order of the asymptotic expansion, which yields the following linear nonhomogeneous system:

$$\begin{pmatrix} L_1 & \partial/\partial t \\ \partial/\partial t & L_2 \end{pmatrix} \begin{pmatrix} U_3 \\ V_3 \end{pmatrix} = \begin{pmatrix} Y \\ Z \end{pmatrix}, \tag{24}$$

where

$$Y = 2(U_1^2 + V_1^2)U_1 + 4U_0(3U_1U_2 + V_1V_2) - V_{2\tau} - 2\rho V_2, \tag{25a}$$

$$Z = 2(U_1^2 + V_1^2)V_1 + 4U_0V_1U_2 + 4U_0U_1V_2 + U_{2\tau} + 2hV_1, \tag{25b}$$

and U_1, V_1, U_2 and V_2 are as in (12) and (15). The solvability condition for equation (24) involves coefficients of the resonant harmonic; we denote them y and z:

$$\begin{pmatrix} Y \\ Z \end{pmatrix} = \begin{pmatrix} y(x,\tau) \\ z(x,\tau) \end{pmatrix} \mathrm{e}^{\mathrm{i}\omega_c t} + \text{c.c.} + (\text{other harmonics}). \tag{26}$$

A bounded solution exists only if

$$\int_{-\infty}^{\infty} (yu_c + zv_c)\,\mathrm{d}x = 0. \tag{27}$$

After some algebra this solvability condition can be reduced to an equation for the complex amplitude of the soliton's perturbation:

$$\alpha\left(\frac{\mathrm{d}^2 a}{\mathrm{d}\tau^2} + 2\rho\frac{\mathrm{d}a}{\mathrm{d}\tau} + \rho^2 a\right) = \beta h a - \zeta|a|^2 a. \tag{28}$$

Here

$$\alpha = -\int_{-\infty}^{+\infty} (u_c v_1 + v_c u_1)\,\mathrm{d}x, \tag{29}$$

$$\beta = 2\int_{-\infty}^{+\infty} v_c^2\,\mathrm{d}x, \tag{30}$$

$$\zeta = -2\int_{-\infty}^{+\infty} (3u_c^4 + 2u_c^2 v_c^2 + 3v_c^4)\,\mathrm{d}x - 4\int_{-\infty}^{+\infty} U_0[3u_c^2(u_0 + u_2) + v_c^2(u_0 - u_2) + 2u_c v_c v_2]\,\mathrm{d}x. \tag{31}$$

In the derivation of the linear part of equation (28) we used the relations

$$\int_{-\infty}^{+\infty} u_c v_\gamma\,\mathrm{d}x = \int_{-\infty}^{+\infty} v_c u_\gamma\,\mathrm{d}x = \int_{-\infty}^{+\infty} u_c v_1\,\mathrm{d}x = \int_{-\infty}^{+\infty} v_c u_1\,\mathrm{d}x;$$

these follow from (9), (17) and (18).

The coefficient β is manifestly positive. Since the oscillatory instability is expected to set in for supercritical values of H, i.e. for $h > 0$, we expect the coefficient α to be positive as well. Finally, the coefficient ζ involves complex functions u_2 and v_2 and therefore, is complex-valued. Using equation (19) in equation (31) one can readily find the imaginary part of this coefficient:

$$\mathrm{Im}\,\zeta = 2k_c\frac{H_c^2 + 4\omega_c^2 + H_c\sqrt{H_c^2 + 4\omega_c^2}}{\omega_c^2}|\mathcal{R}|^2 > 0. \tag{32}$$

The eigenvalue problem (9) and nonhomogeneous equations (16)–(19) were solved numerically. (The details have been relegated to the appendix.) We have found the following values for the coefficients occurring in the reduced amplitude equation (28):

$$\begin{aligned} &\alpha = 1.3297, \qquad \beta = 1.6447, \\ &\mathrm{Re}\,\zeta = (7.5555 \pm 0.0005)\times 10^{-2}, \qquad \mathrm{Im}\,\zeta = (1.59 \pm 0.04)\times 10^{-3}. \end{aligned} \tag{33}$$

3. Reduced amplitude equations for the Hopf bifurcation

In this section we derive the reduced amplitude equation governing nonlinear evolutions beyond the Hopf bifurcation. The Hopf bifurcation occurs when a pair of complex-conjugate linearized eigenvalues crosses the imaginary axis at $\lambda = \mathrm{i}\Omega_c(\Gamma)$ (see figures 2(*a*) and (*c*)). As we have already mentioned, this bifurcation takes place in the *strongly* dissipative case, i.e. for $H = H_c(\Gamma)$ with *finite* Γ†. We expand the fields as in equations (11) and (12):

$$U = U_0(x) + \epsilon[a(\tau)\mathrm{e}^{\mathrm{i}\Omega_c t} + a^*(\tau)\mathrm{e}^{-\mathrm{i}\Omega_c t}]f_c(x) + \sum_{n=2}^{\infty}\epsilon^n U_n(x, t, \tau), \tag{34a}$$

† In the previous two sections we used the notation H_c for the value of H for which the eigenvalues ω_a and ω_b merge and become complex. That previous H_c would be called $H_c(0)$ in the context of this section.

$$V = \mathrm{i}\epsilon[a(\tau)\mathrm{e}^{\mathrm{i}\Omega_c t} - a^*(\tau)\mathrm{e}^{-\mathrm{i}\Omega_c t}]g_c(x) + \sum_{n=2}^{\infty}\epsilon^n V_n(x,t,\tau), \tag{34b}$$

with, however, a different time scaling:

$$\tau = \epsilon^2 t.$$

We also assume that

$$H = H_c(\Gamma) + \epsilon^2\hat{h}.$$

In equations (34) f_c and g_c are *complex* eigenfunctions of the operator (6) associated with the eigenvalue $\Omega = \Omega_c(\Gamma)$ and arising for $H = H_c(\Gamma)$. The second-order correction terms become

$$U_2 = |a|^2 f_0(x) + 2\,\mathrm{Re}\{a^2\mathrm{e}^{2\mathrm{i}\Omega_c t} f_2(x)\},$$
$$V_2 = |a|^2 g_0(x) + 2\,\mathrm{Re}\{\mathrm{i}a^2\mathrm{e}^{2\mathrm{i}\Omega_c t} g_2(x)\},$$

where f_0 and g_0 are real functions satisfying the nonhomogeneous system

$$\begin{pmatrix} L_1 & 2\Gamma \\ 0 & L_2 \end{pmatrix}\begin{pmatrix} f_0 \\ g_0 \end{pmatrix} = 4U_0\begin{pmatrix} 3|f_c|^2 + |g_c|^2 \\ \mathrm{i}(f_c^* g_c - g_c^* f_c) \end{pmatrix}, \tag{35}$$

and $\{f_2, g_2\}$ is a complex solution to

$$\begin{pmatrix} L_1 & 2\mathrm{i}\Gamma - 2\Omega_c \\ -2\Omega_c & L_2 \end{pmatrix}\begin{pmatrix} f_2 \\ g_2 \end{pmatrix} = 2U_0\begin{pmatrix} 3f_c^2 - g_c^2 \\ 2f_c g_c \end{pmatrix}. \tag{36}$$

Both equations (35) and (36) exhibit nonhomogeneous solutions exponentially decaying as $|x| \to \infty$ because the corresponding *homogeneous* solutions are all unbounded—with a single exception of the translational mode $f_T(x) = \tanh x\,\mathrm{sech}\,x$, $g_T(x) = 0$ which we have already mentioned in section 2. As for the continuous spectrum of the operator (6), it consists of Ω with $\Omega(\Omega - 2\mathrm{i}\Gamma) = \omega^2$, where ω is real and $\omega^2 > 1 - 2H_c$. Consequently, no real Ω belong to the continuous spectrum.

Thus, we proceed to the third-order approximation along the lines of section 2 and find the complex Landau equation for the amplitude $a(\tau)$:

$$\hat{\alpha}\frac{\mathrm{d}a}{\mathrm{d}\tau} = \hat{\beta}\hat{h}a - \hat{\zeta}|a|^2 a. \tag{37}$$

Here the complex coefficients $\hat{\alpha}$, $\hat{\beta}$, and $\hat{\zeta}$ are expressible through the functions f_c, g_c and f_0 to g_2:

$$\hat{\alpha} = (\Gamma + \mathrm{i}\Omega_c)\int_{-\infty}^{+\infty} f_c g_c\,\mathrm{d}x,$$

$$\hat{\beta} = (\Omega_c - 2\mathrm{i}\Gamma)\int_{-\infty}^{+\infty} g_c^2\,\mathrm{d}x,$$

$$\begin{aligned}\hat{\zeta} = -\Omega_c\int_{-\infty}^{+\infty}(3|f_c|^2 f_c^2 + |f_c|^2 g_c^2 + |g_c|^2 f_c^2 + 3|g_c|^2 g_c^2)\,\mathrm{d}x \\ +2\mathrm{i}\Gamma\int_{-\infty}^{+\infty}(3|g_c|^2 g_c^2 + 2|f_c|^2 g_c^2 - |g_c|^2 f_c^2)\,\mathrm{d}x \\ -2\Omega_c\int_{-\infty}^{+\infty} U_0\{3f_c^2 f_0 + 3|f_c|^2 f_2 + (f_c g_c^* + f_c^* g_c)g_2 + g_c^2 f_0 - |g_c|^2 f_2\}\,\mathrm{d}x \\ +4\mathrm{i}\Gamma\int_{-\infty}^{+\infty} U_0(g_c^2 f_0 - |g_c|^2 f_2 - \mathrm{i}f_c g_c g_0 + f_c^* g_c g_2)\,\mathrm{d}x.\end{aligned}$$

The amplitude equation (37) is a normal form of the Hopf bifurcation occuring in finite-dimensional dissipative systems (see e.g. [20]).

We conclude this section by a comment on the correspondence between 'large Γ' and 'small Γ' amplitude equations, i.e. equations (37) and (28). Sending $\Gamma \to 0$, we have

$$\begin{pmatrix} f_c \\ g_c \end{pmatrix} = \begin{pmatrix} u_c \\ v_c \end{pmatrix} + \mathrm{i}\Gamma \begin{pmatrix} u_\gamma \\ v_\gamma \end{pmatrix} + \mathrm{O}(\Gamma^2) \tag{38}$$

and the coefficients of equation (37) become

$$\hat{\alpha} = \Gamma\Omega_c\alpha, \qquad \hat{\beta} = \frac{\Omega_c}{2}\beta, \qquad \hat{\zeta} = \frac{\Omega_c}{2}\zeta. \tag{39}$$

On the other hand, when $\rho \to \infty$ the amplitude equation (28) becomes overdamped and the $a_{\tau\tau}$ term can be discarded. This converts equation (28) into the first-order equation†

$$2\alpha\rho a_\tau = (\beta h - \alpha\rho^2)a - \zeta|a|^2 a, \tag{40}$$

which coincides with (37), (39) after we have made the identification $\hat{h} = h - \alpha\rho^2/\beta$, or, equivalently,

$$H_c(\Gamma) = H_c(0) + \frac{\alpha}{\beta}\Gamma^2. \tag{41}$$

As an aside remark we note that equation (41) can be rewritten as

$$\mathfrak{h}_c(\gamma) = \mathfrak{h}_c(0) + \frac{\alpha}{\beta}\frac{\gamma^2}{1 + \mathfrak{h}_c(0)} = 0.063\,596 + 0.760\,13\gamma^2, \tag{42}$$

which gives a small-γ approximation for the upper boundary of the stationary soliton's stability domain.

4. Finite-dimensional supercritical dynamics

4.1. Linear stage

The linear stability properties of the stationary soliton of the NLS equation (4) are exactly reproduced by the reduced amplitude equation, equation (28). In terms of equation (28) the linear stage of instability can be described by discarding the cubic term. This yields

$$a(\tau) = a_0 \mathrm{e}^{\mu\tau}, \qquad \mu = -\rho \pm \sqrt{\frac{\beta h}{\alpha}}. \tag{43}$$

In the *undamped* case ($\rho = 0$) equation (43) implies that the oscillatory instability sets in immediately as h becomes greater than zero. This is in exact correspondence with figure 1(*a*) where the instability is seen to arise when two imaginary eigenvalues $\lambda_a = \mathrm{i}\omega_a$ and $\lambda_b = \mathrm{i}\omega_b$ merge for $H = H_c$ (or, equivalently, for $h = 0$) and then split up and diverge from the imaginary axis. In the *weakly dissipative* case ($\rho \neq 0$) the coalescing eigenvalues have a negative real part at the point of their merger and so the instability sets in not when they coalesce but later, when one of the diverging eigenvalues crosses the imaginary axis. This happens at $h = h_c \equiv \alpha\rho^2/\beta$ and again, this threshold value is exactly reproduced by the threshold value of the reduced equation (which is straightforward from (43)).

Finally, in the *strongly* dissipative case the merger of the eigenvalues and the imaginary axis crossing occur for two widely separated values of H. Here we deal with the conventional Hopf bifurcation; in this case the second-order amplitude equation does not apply and should be replaced by the complex Landau equation, equation (37).

† A more formal way to obtain a first-order equation consists in transforming to $\tilde{\tau} = \tau/\rho$ and then sending $\rho \to \infty$.

4.2. Energy considerations

The undamped parametrically driven NLS equation (1) has two conserved quantities, the field momentum and energy. The eigenfunctions associated with the soliton's internal oscillation modes are symmetric in x and so these oscillations do not affect the value of the momentum. Consequently, energy is the only relevant integral in the present context. Although in the dissipative case ($\gamma \neq 0$) energy is not conserved, it remains a useful characteristic of the wave field in this case as well. For $\gamma \neq 0$ the local energy balance equation follows from equations (4):

$$\frac{\partial \mathcal{E}}{\partial t} + \frac{\partial F_{\mathcal{E}}}{\partial x} = -2\Gamma D_{\mathcal{E}}, \tag{44}$$

where

$$\mathcal{E} = \tfrac{1}{2}[U_x^2 + V_x^2 + U^2 + (1-2H)V^2 - (U^2+V^2)^2] \tag{45}$$

is the energy density,

$$F_{\mathcal{E}} = U_x V_{xx} - U_{xx} V_x + UV_x - (1-2H)VU_x + 2(U^2+V^2)(U_x V - UV_x) \tag{46}$$

the associated flux, and

$$D_{\mathcal{E}} = V_x^2 + (1-2H)V^2 - 2(U^2+V^2)V^2 \tag{47}$$

is the density of the dissipative function. Substituting the asymptotic expansion (11) in equation (45) and integrating over x gives a total energy of the nonlinear wave field:

$$E = \int_{-\infty}^{+\infty} \mathcal{E}\,\mathrm{d}x = E_0 + \epsilon^2 E_2 + \epsilon^3 E_3 + \mathrm{O}(\epsilon^4), \tag{48}$$

where E_0 is the energy of the unperturbed soliton ($E_0 = 2/3$), and E_2, E_3, etc are corrections due to the small localized perturbation. It follows from equations (9) and (11) that

$$E_2 = \omega_c I_c |a|^2,$$

where I_c is the quadratic functional (23) evaluated at the critical eigenvector $\{u_c, v_c\}$: $I_c = I[u_c, v_c]$. The quadratic form I is positive for the eigenmode $\{u_b, v_b\}$ which detaches from the edge of the continuous spectrum and negative for the eigenvector $\{u_a, v_a\}$ arising from the broken phase invariance (see figure 3). Therefore, the eigenfunction $\{u_b, v_b\}$ always brings a positive contribution to the energy of the nonlinear field, while the contribution of the mode $\{u_a, v_a\}$ is always negative. At the resonance ($H = H_c$) the two contributions cancel each other and the second-order correction E_2 vanishes according to equation (22). The merger of two modes of the opposite energetic contents produces the oscillatory instability of the stationary soliton (2). At the resonance, the asymptotic expansion (48) must be extended to include the third-order correction, for which we obtain

$$E_3 = \mathrm{i}\alpha\omega_c \left(a \frac{\mathrm{d}a^*}{\mathrm{d}\tau} - a^* \frac{\mathrm{d}a}{\mathrm{d}\tau} \right) \tag{49}$$

with α is as in equation (29). Finally, integrating equation (44) over x and keeping terms up to ϵ^3 in the expansion (48) we find the rate of change of the energy of the localized wave field:

$$\frac{\mathrm{d}E_3}{\mathrm{d}\tau} = -2\rho E_3 - 2\omega_c \,\mathrm{Im}\,\zeta\, |a|^4. \tag{50}$$

(This equation, with E_3 defined by (49), can also be derived directly from the reduced amplitude equation (28).) The equation (50) shows that the soliton is suffering two types of energy losses: the dissipative losses described by the first term on the right-hand side and losses due to the emission of radiation waves described by the second term.

4.3. Effective particle representation

It appears useful to interpret the reduced amplitude equation (28) as the equation of motion of a fictitious classical particle. In terms of the vector $\boldsymbol{r} \equiv \{\mathrm{Re}\, a, \mathrm{Im}\, a\}$, equation (28) becomes

$$\ddot{\boldsymbol{r}} + 2\rho\dot{\boldsymbol{r}} - \eta\boldsymbol{r} + gr^2\boldsymbol{r} = qr^2\boldsymbol{r} \times \hat{\boldsymbol{z}}, \tag{51}$$

where we have defined

$$g = \frac{\mathrm{Re}\,\zeta}{\alpha} \approx 0.0568, \qquad q = \frac{\mathrm{Im}\,\zeta}{\alpha} \approx 0.0012,$$

and

$$\eta = \frac{\beta}{\alpha}h - \rho^2.$$

(The control parameter η is positive in the supercritical region.) Next, $\hat{\boldsymbol{z}}$ is a unit vector in the vertical direction; $r \equiv |\boldsymbol{r}|$, and the overdot indicates differentiation with respect to τ. Equation (51) describes a particle in a mexican hat-shaped radially-symmetric potential

$$\mathcal{U}(r) = -\frac{\eta}{2}r^2 + \frac{g}{4}r^4, \tag{52}$$

subject to the constant friction with coefficient 2ρ and clockwise r-dependent torque $-qr^4\hat{\boldsymbol{z}}$. Two quantities useful for the analysis are the angular momentum

$$l = [\boldsymbol{r} \times \dot{\boldsymbol{r}}]\Big|_z = \frac{\mathrm{i}}{2}(a\dot{a}^* - a^*\dot{a}), \tag{53}$$

and the Hamiltonian

$$\mathcal{H} = \frac{\dot{r}^2}{2} + \frac{l^2}{2r^2} + \mathcal{U}(r). \tag{54}$$

In terms of l and $\mathcal{H}$ the vector equation (51) can be rewritten as

$$\dot{l} = -2\rho l - qr^4, \tag{55}$$

$$\dot{\mathcal{H}} + 2\rho\dot{r}^2 = -2\rho\frac{l^2}{r^2} - qlr^2. \tag{56}$$

Notice that l coincides, up to a constant factor, with the third-order correction to the soliton's energy, equation (49):

$$E_3 = 2\alpha\omega_c l. \tag{57}$$

Accordingly, equation (55) is simply the equation of the soliton's energy variation, equation (50), rewritten in terms of the angular momentum of the fictitious particle.

4.4. Conservative case ($\rho = 0$)

First we consider the case $\rho = 0$. Although the NLS equation is conservative in this case (i.e. the total energy (48) does not change with time), the motion of the effective particle is not. According to equation (50), in the conservative case the solitary wave evolves in such a way that the energy E_3 is decreasing at all times due to the radiation losses. In the language of the fictitious particle this means that the angular momentum is always growing towards minus infinity due to the nonzero clockwise torque. As we will see, the consequence of this in the unstable region $h > 0$ is that the dynamical system (28) has no bounded trajectories and the amplitude a has to grow indefinitely.

If there were no external torque ($q = 0$), both l and $\mathcal{H}$ would be conserved and consequently, the fictitious particle would perform quasiperiodic oscillations in the ring $R_1 < r < R_2$. Here R_1^2 and R_2^2 are the two positive roots of the cubic equation

$$\mathcal{U}_{\rm eff}(R^2) = \mathcal{H}, \qquad \mathcal{U}_{\rm eff}(R^2) = \frac{l^2}{2R^2} - \frac{\eta}{2}R^2 + \frac{g}{4}R^4. \tag{58}$$

Let now q be nonzero but so small that we can still regard the particle as being trapped in an effective radially-symmetric potential well (58), with l, the width of the centrifugal barrier, and the energy of the particle slowly changing with time:

$$\dot{l} = -qr^4, \qquad \dot{\mathcal{H}} = -qlr^2. \tag{59}$$

Assume first that the initial value of the angular momentum is negative: $l(0) < 0$. Then l will grow in magnitude remaining negative all the time, and the energy $\mathcal{H}$ will also grow. It is not difficult to show that as a result of this, the inner and outer radii of the ring (the so-called apsidal distances) will grow as well. Indeed, differentiating the identity $\mathcal{U}_{\rm eff}(R_i^2) = \mathcal{H}$ and then using equation (59) and the representation

$$\frac{l^2}{2R^2} - \frac{\eta}{2}R^2 + \frac{g}{4}R^4 - \mathcal{H} = \frac{g}{4}\frac{(R^2 - R_1^2)(R^2 - R_2^2)(R^2 + R_3^2)}{R^2}, \tag{60}$$

one finds

$$\frac{\rm d}{{\rm d}\tau}R_i^2 = -\frac{4qlr^2}{g}\frac{|R_i^2 - r^2|}{(R_2^2 - R_1^2)(R_i^2 + R_3^2)}, \qquad i = 1, 2, \tag{61}$$

which is $\geqslant 0$ for $l < 0$. Intuitively it is quite clear from (61) that the inner circle of the ring will grow faster than the outer circle; this claim can be readily justified by comparing the increments incurred by R_1 and R_2 in one half-period of oscillation, i.e. as the particle travels from R_1 to R_2. Consequently, the particle will spin around the origin within an adiabatically expanding and narrowing annular well. (By 'narrowing' we mean that the *width* of the ring will be decreasing.)

Assume now that the initial value of the angular momentum is positive: $l(0) > 0$. In this case both l and $\mathcal{H}$ will initially decrease, and, according to (61), the trajectory will be sandwiched between two adiabatically shrinking circles: ${\rm d}R_{1,2}/{\rm d}\tau < 0$. Eventually l will become negative, and the evolution will cross over to the previous scenario.

The motion remains adiabatic as long as the width of the ring, $R_2 - R_1$, is much larger than the increments incurred by $R_1(\tau)$ and $R_2(\tau)$ during one half-period of oscillation. To find the region of applicability of this condition, we consider the stage where the Hamiltonian is already so large that

$$\frac{\eta^2}{g\mathcal{H}} \ll \frac{1}{3}. \tag{62}$$

We also assume, for simplicity of calculations, that†

$$\sigma \equiv \frac{gl^4}{\mathcal{H}^3} \ll \left(\frac{4}{3}\right)^3; \tag{63}$$

then the roots R_i are given by simple expressions

$$R_1^2 \approx \frac{l^2}{2\mathcal{H}}, \qquad R_2^2 \approx R_3^2 \approx \left(\frac{4\mathcal{H}}{g}\right)^{1/2}. \tag{64}$$

† The particular numerical values on the right-hand side of (62) and (63) are suggested simply by the fact that for $\eta^2/g\mathcal{H} < \frac{1}{3}$ and $\sigma < (\frac{4}{3})^3$, the roots of the cubic equation can be found as convergent series in $(\eta^2/g\mathcal{H})$ and σ.

Notice that in view of the inequality (63), $R_1/R_2 \ll 1$. (More precisely, $R_1^2/R_2^2 \ll 2/\sqrt{27}$). From (61) it follows that the velocity of expansion (or contraction) of the inner circle of the ring satisfies

$$|\dot{R}_1| < \frac{2q|l|}{g}\frac{\sqrt{r^2 - R_1^2}}{R_1 R_2},$$

where we have used the fact that $R_3 \approx R_2 \gg R_1$. On the other hand, the radial velocity of the particle is given by

$$|\dot{r}| = \sqrt{\frac{g(r^2 - R_1^2)(R_2^2 - r^2)(r^2 + R_3^2)}{2r^2}},$$

whence the increment in R_1 is

$$|\Delta R_1| = \left| \int_{R_1}^{R_2} \dot{R}_1 \frac{\mathrm{d}r}{\dot{r}} \right| < q\left(\frac{g}{2}\right)^{-3/2} \frac{|l|\sqrt{R_2^2 - R_1^2}}{R_1 R_2^2}.$$

Using (64), we obtain

$$\frac{|\Delta R_1|}{R_2 - R_1} < \frac{2q}{g},$$

and since our $2q/g \approx 0.04$, we conclude that the adiabaticity condition $|\Delta R_1| \ll R_2 - R_1$ is in place. In a similar way one obtains

$$|\Delta R_2| < \sqrt{2} q g^{-3/2} \frac{|l|\sqrt{R_2^2 - R_1^2}}{R_2^3},$$

and making use of equations (64), this becomes $q|l| < 2(g\mathcal{H})^{3/4}$. Therefore, in order to ensure that $|\Delta R_2| \ll R_2 - R_1$, it is sufficient to require that the dimensionless quantity σ, equation (63), be much smaller than $(2g/q)^4 \sim 8 \times 10^7$. The latter is automatically satisfied if we impose the condition (63).

As $\mathcal{H}$ and $(-l)$ grow and the ring expands and its width narrows, the quotient σ will receive a positive increment after each period of oscillation. Quantitatively, the increment incurred in a half-period is

$$\Delta\sigma = \int_{R_1}^{R_2} \dot{\sigma}\frac{\mathrm{d}r}{\dot{r}} > \frac{(\sqrt{2} - 1)\pi q}{2g}\sigma. \tag{65}$$

On the other hand, it takes the particle less than $\frac{\pi}{2}(g\mathcal{H})^{-1/4}$ units of time to travel from R_1 to R_2. Consequently, the average growth rate can be estimated as

$$\langle\dot{\sigma}\rangle \equiv \frac{\int_{R_1}^{R_2} \dot{\sigma}\frac{\mathrm{d}r}{\dot{r}}}{\int_{R_1}^{R_2} \frac{\mathrm{d}r}{\dot{r}}} \gg \frac{3^{1/4}(\sqrt{2} - 1)q}{g} b^{1/2}\sigma^{5/4}, \tag{66}$$

where we have used the inequality (62). This means that σ will grow at least as fast as $1/(\tau_0 - \tau)^4$ (with τ_0 determined by the initial value of σ). Eventually the inequality (63) will be no longer valid, and oscillations in an adiabatically growing ring will be replaced by a regime of a faster, almost monotonic growth. (What happens is that the annular well becomes so narrow and expands so fast, that it simply 'pulls' the particle along.)

It is not difficult to realize that this latter regime is self-similar. Since $\eta/(gr^2) \to 0$, the term with η can be neglected in equation (56) and the growing solution of the resulting system is simply

$$r = \frac{r_1}{\tau_0 - \tau}, \qquad l = -\frac{l_1}{(\tau_0 - \tau)^3}, \tag{67a}$$

where

$$r_1 = \frac{3}{\sqrt{2}}\frac{\sqrt{g}}{q}\left(1+\sqrt{1+\frac{8}{9}\frac{q^2}{g^2}}\right)^{1/2} \approx 3\frac{\sqrt{g}}{q} \approx 6.0\times 10^2, \tag{67b}$$

and

$$l_1 = \frac{q}{3}r_1^4 \approx 5.0\times 10^7. \tag{67c}$$

The energy grows as

$$\mathcal{H} = \frac{\mathcal{H}_1}{(\tau_0-\tau)^4}, \qquad \mathcal{H}_1 = \frac{q^2}{12}r_1^6 \approx 5.4\times 10^6, \tag{68}$$

while the quotient σ remains constant:

$$\sigma = \frac{64g}{3q^2r_1^2} \approx \left(\frac{4}{3}\right)^3 \approx 2.37. \tag{69}$$

Figures 4(*a*) and (*c*) show results of the numerical simulation of the finite-dimensional system (28) (equivalently, equation (51)) with the initial conditions satisfying equations (62) and (63). For both negative and positive $l(0)$ the evolution starts with a long transient where the particle performs oscillations in an adiabatically expanding or contracting ring. When $l(0) > 0$, the ring is initially shrinking (this phase is not very clearly seen in the plot) but then starts expanding. When $l(0) < 0$, the shrinking phase is absent and because of that, the evolution in this case is approximately 10 time units ahead of the one for $l(0) > 0$. The exponent σ is seen to tend to the similarity value of 2.37; this indicates that the trajectory is attracted to the self-similar regime (67).

It is important to emphasize here that the inequalities (62), (63) are sufficient but in no way necessary for the adiabatic transient to occur. (In fact, the only role of equations (62), (63) was to simplify calculations.) In figures 4(*b*) and (*d*) we display trajectories of the particle with the initial conditions which do not satisfy (62), (63). Similarly to the previous case, initially the particle is oscillating within an adiabatically changing ring (i.e. $\Delta R_i \ll R_2 - R_1$) but then escapes to infinity along a self-similar trajectory ($\sigma \to 2.37$). As in the previous case, the duration of the transient depends on the sign of $l(0)$: for $l(0) < 0$ the ring starts expanding straight away whereas for $l(0) > 0$, the ring first contracts until the sense of rotation of the particle is reversed, and only then starts inflating. In terms of the full, nonreduced NLS equation this means that initial perturbations 'pushing' the soliton towards smaller values of E will trigger a much faster decay of the unstable soliton than those bringing positive contribution to its energy.

Thus we may conclude that in the conservative case, the oscillatory instability bifurcation does not give rise to a stably oscillating soliton. The reason for this is the emission of a strong second-harmonic radiation. Because of the radiation, the trajectory of the soliton's perturbation in its internal space is always unbounded. Provided the initial perturbation $|a(0)|$ is not very large, the evolution of instability starts with adiabatically growing oscillations which then transform into a regime of rapid self-similar growth.

4.5. Weakly dissipative case (finite ρ)

Adding a weak damping can hinder radiations from freely escaping from the oscillating soliton. According to equation (55) this can result in the angular momentum of the fictitious particle settling to a constant value

$$l_\pm = -\frac{q}{2\rho}r_\pm^4, \tag{70}$$

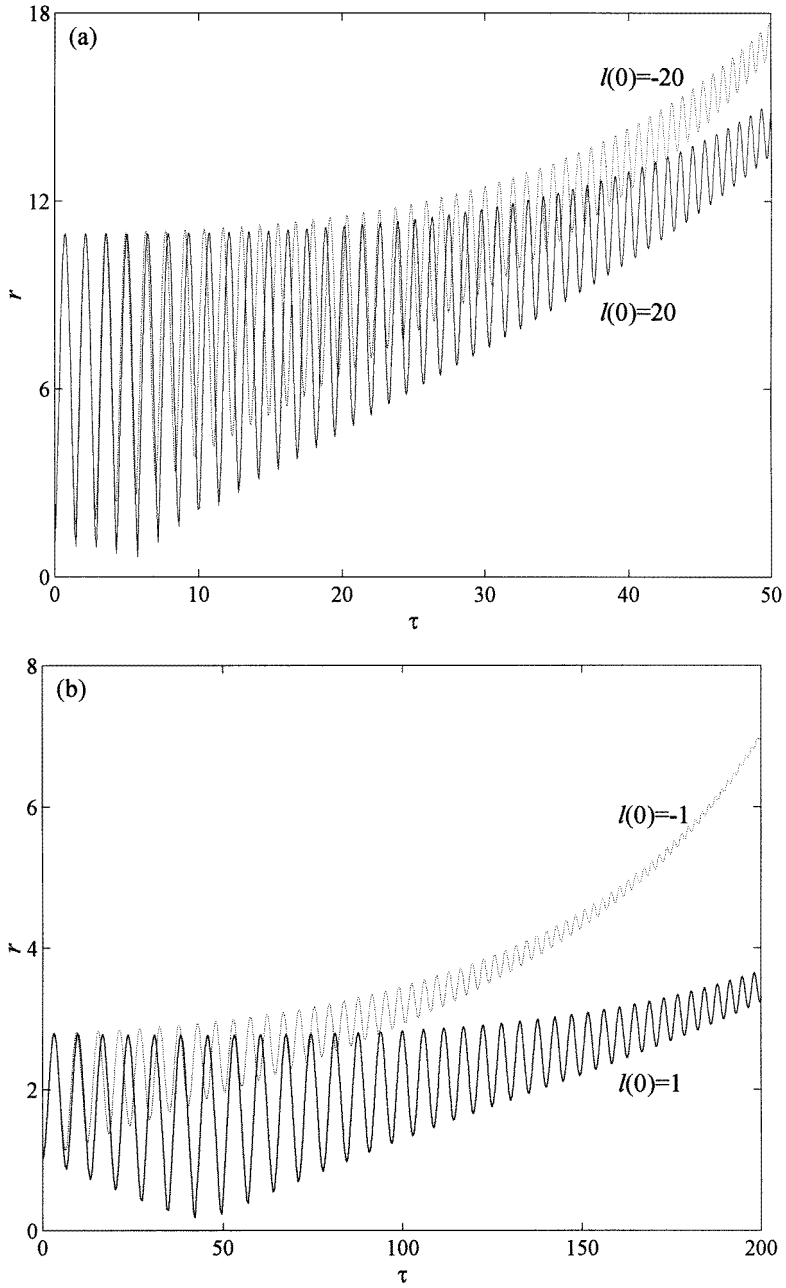

Figure 4. The motion of the undamped classical particle as obtained by numerical simulations of equation (51): the radial position of the particle (*a*), (*b*) and the exponent $\sigma = gl^4/\mathcal{H}^3$ (*c*), (*d*). In these plots $h = 0.1$ ($\eta = 0.1237$); in all four runs the initial radial position was $r(0) = 1$ and the initial radial velocity $\dot{r}(0) = 0$. On (*a*), (*c*) the initial angular momentum is $l(0) = \pm 20$ which gives $\eta^2/g\mathcal{H}(0) \sim 10^{-3}$ and $\sigma(0) \sim 10^{-3}$ so that the inequalities (62), (63) hold true. On the contrary, neither of these inequalities is satisfied for the evolutions shown on (*b*), (*d*); these start with $l(0) = \pm 1$ which gives $\eta^2/g\mathcal{H}(0) \approx 0.6$ and $\sigma(0) \approx 0.6$.

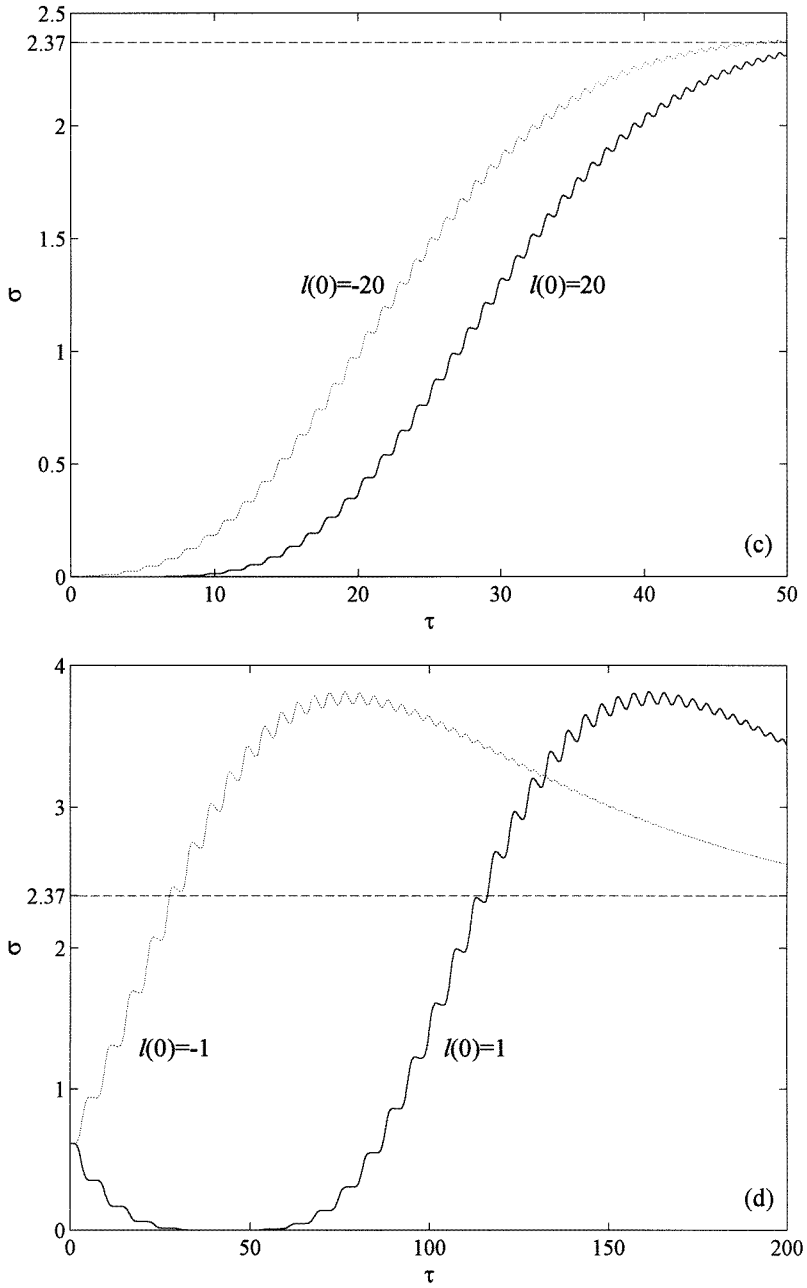

Figure 4. (Continued)

where the radius can adopt one of the two values:

$$r_{\pm}^2 = \frac{2\rho^2}{q^2}\left(g \pm \sqrt{g^2 - \frac{q^2\eta}{\rho^2}}\right). \tag{71}$$

The corresponding circular orbits of equation (51) have the form

$$a = r_{\pm}\exp(\mathrm{i}\nu_{\pm}\tau), \tag{72}$$

with the angular velocities given by

$$\nu_{\pm} = -\frac{q}{2\rho}r_{\pm}^2. \tag{73}$$

Both closed trajectories exist for $g > 0$ which is in place in the case at hand. In terms of the parametrically driven NLS equation, equations (71)–(73) describe two periodically oscillating solitons different in the amplitude and frequency of oscillation.

The soliton with the smaller amplitude of oscillation, $|a| = r_{-}$, softly bifurcates from the stationary soliton at the onset of the oscillatory instability, $h = h_c = \alpha\rho^2/\beta$. As h is increased, it merges with the second oscillating soliton ($|a| = r_{+}$) at the turning point

$$\overline{h} = h_c\left[1 + \left(\frac{g}{q}\right)^2\right]. \tag{74}$$

The value $\overline{h}$ is the upper boundary of the domain of existence of the two circular orbits (71)–(73). Intuitively, it is quite clear that the orbit r_{-} should be stable and r_{+} unstable; to verify this conjecture, we add a small perturbation:

$$a(\tau) = (r_{\pm} + \mathrm{e}^{\mu\tau}\delta a)\exp(\mathrm{i}\nu_{\pm}\tau), \qquad |\delta a/r_{\pm}| \ll 1. \tag{75}$$

Substituting into (51) and linearizing with respect to δa yields a characteristic equation for the exponent μ:

$$\mu(\mu^3 + c_1\mu^2 + c_2\mu + c_3) = 0, \tag{76}$$

where $c_1 = 4\rho > 0$,

$$c_2 = 4\rho^2 + 2gr_{\pm}^2 + 4\nu_{\pm}^2 > 0,$$

and

$$c_3 = 4\rho(gr_{\pm}^2 - 2\nu_{\pm}^2) = \mp 4r_{\pm}^2\sqrt{g^2\rho^2 - q^2\eta}.$$

Using the Routh–Hurvitz test, one may readily check that apart from the trivial translational root $\mu = 0$, equation (76) always has two roots with negative real parts. The fourth root is positive for $c_3 < 0$ and negative otherwise; that is, we have a stable root for $r = r_{-}$ and unstable one for $r = r_{+}$. Thus the oscillating soliton with the larger amplitude of oscillations is unstable and the one with the smaller amplitude is stable within our asymptotic approximation.

All trajectories of the fictitious particle will either be attracted to the stable circular orbit r_{-}, l_{-} or escape to infinity along a self-similar trajectory similar to the one arising in the undamped situation. This self-similar solution is given by the same equations (67) as in the $\gamma = 0$ case. We are not discussing basins of attraction of the above solutions; this analysis can be performed along the lines of the previous section. In this paper we confine ourselves to displaying only several characteristic transients (figure 5).

In all our experiments the radial component of velocity was initially zero: $\dot{r}(0) = 0$. In the first simulation the initial angular momentum is negative and $|l(0)|$ and $r(0)$ are chosen in such a way that in the first place, $qr^4(0) > 2\rho|l(0)|$, and in the second, the ring of admissible motions is wider than both stationary circular orbits: $R_1(0) > r_{+}$. (We remind that $R_1(\tau)$

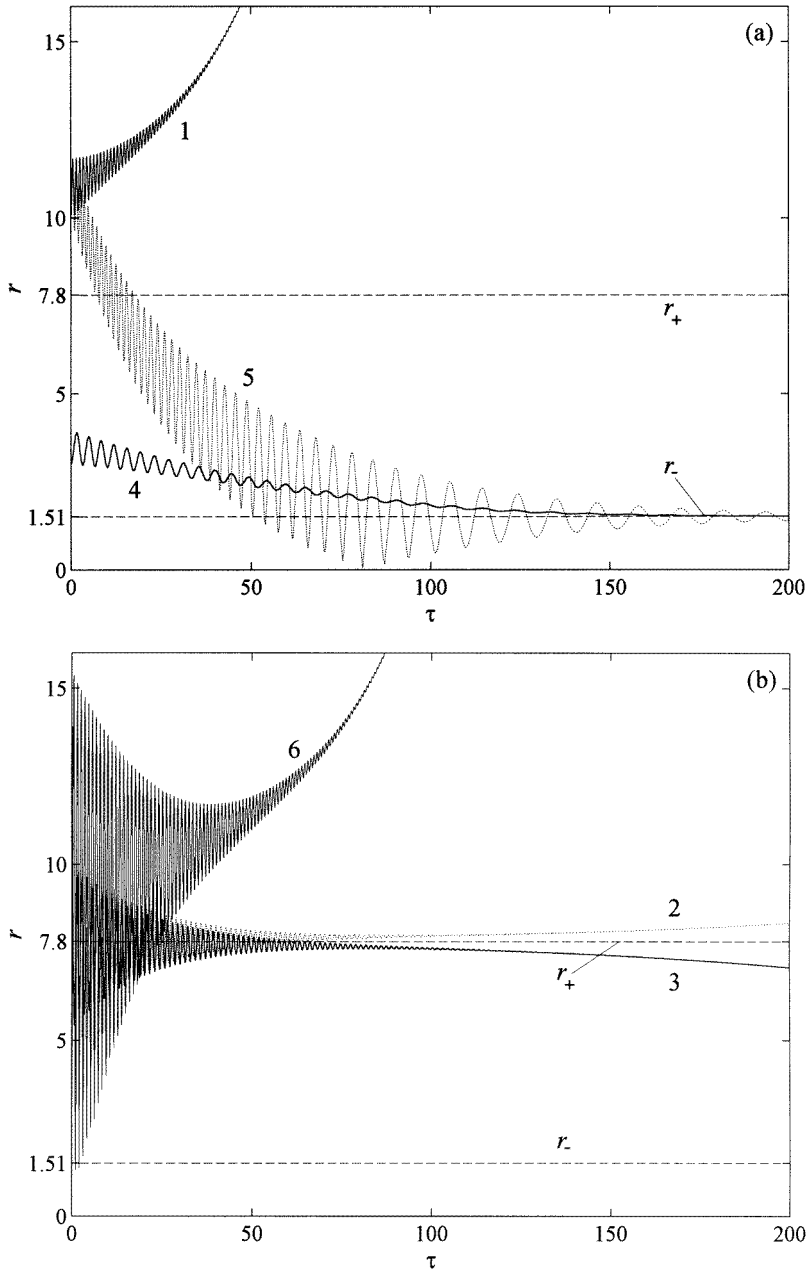

Figure 5. Numerical simulations of the damped fictitious particle, equation (51). Here $\rho = 0.02$ and $\eta = 0.1237$; the corresponding stationary orbits are $r_- = 1.51$ (stable) and $r_+ = 7.80$ (unstable). Curve 1 starts with $r(0) = 10$, $l(0) = -300$ and curve 5 has $r(0) = 10$, $l(0) = +300$; in both cases the corresponding $R_1(0) = 10$, and $R_2(0) = 11.7$. Curve 2 has $r(0) = 9.97$, $l(0) = -99.40$; the apsidal distances in this case are $R_1(0) = 5.33$, and $R_2(0) = 9.97$. Curve 3 starts with $r(0) = 9.80$ and $l(0) = 96.04$; the corresponding $R_1(0) = 5.31$ and $R_2(0) = 9.80$. After visiting the unstable orbit r_+, the curve 2 escapes to infinity while the curve 3 settles to the stable orbit r_-. The initial conditions for the curve 4 are $r(0) = 3$ and $l(0) = -9$; hence $R_1(0) = 3$, $R_2(0) = 4$. Curve 6 has $r(0) = 0.5$, $l(0) = +20$, the corresponding $R_1(0) = 0.5$, $R_2(0) = 15.5$.

and $R_2(\tau)$ are defined as roots of equation (58).) In this case the angular momentum starts decreasing further ($\dot{l} < 0$) and equation (55) implies that the height of the centrifugal barrier at any fixed point $r = r_0$ grows as

$$\frac{\mathrm{d}}{\mathrm{d}\tau}\left(\frac{l^2}{2r_0^2}\right) = |l|\frac{qr^4 - 2\rho|l|}{r_0^2}. \tag{77}$$

On the other hand, in view of equation (56) the growth rate of the energy of the particle, $\dot{\mathcal{H}}$, is bounded by $|l|(qr^4 - 2\rho|l|)/r^2$ which is smaller than (77) provided $r_0 < R_1(\tau)$. Consequently, the centrifugal barrier grows faster than $\mathcal{H}(\tau)$ and the 'window' of admissible motions, $(R_1,\ R_2)$, moves further away from r_+ (curve 1). The particle escapes to infinity.

Initial conditions with $l(0) < 0$ and $qr^4(0) > 2\rho|l(0)|$ do not necessarily give rise to unbounded motions. If the ring of admissible motions is initially smaller than r_+ (i.e. $R_2(0) < r_+$) or contains the orbit r_+ within it (i.e. $R_1(0) < r_+ < R_2(0)$), the expanding ring may lock on to the unstable circular orbit (curves 2 and 3) and then the initial expansion may switch to contraction (curve 3). Finally, such a trajectory will be attracted to the stable orbit r_-.

If $l(0) < 0$ but $qr^4(0) < 2\rho|l(0)|$, both the centrifugal barrier and energy as a whole will decrease and the trajectory will quickly settle to the circular orbit r_- (curve 4).

When the initial angular momentum is positive, the early stage of the evolution will necessarily have to go via the shrinking of the ring, curves 5 and 6. (This is because both l and $\mathcal{H}$ decrease, see equations (55), (56).) Subsequently, *narrow* rings will shrink to the circle r_- (curve 5) whereas the direction of change of the *large-width* rings may reverse and the trajectory escape to infinity (curve 6).

Returning to solutions of the parametrically driven, damped NLS equation (1), we conclude that in the weakly dissipative case the nonlinear evolution of the unstable stationary soliton $\psi_+(X)$ may follow two alternative scenarios. The first one is the formation of a temporally periodic soliton $\psi_\sim(X, T)$; this scenario is in exact agreement with numerical simulations of [4] where stable oscillating solitons were observed. In the vicinity of the bifurcation the soliton $\psi_\sim(X, T)$ oscillates about the 'stationary point' $\psi_+(X)$; that is, the difference $|\psi_\sim - \psi_+|$ is not large. Alternatively, the stationary soliton may undergo a more dramatic transformation described by an unbounded trajectory of the effective particle. The final product of this transformation is beyond the scope of the reduced amplitude equation and the only means to find the resulting attractors seems to be the direct computer simulations of the full, nonreduced NLS (1). Some insight can also be gained from studying the undamped limit ($\gamma = 0$), see section 5 below.

4.6. Strongly dissipative case ($\rho \gg 1$)

As we have demonstrated in section 3, for large ρ the second-order amplitude equation simplifies to the normal form of the Hopf bifurcation, equation (40). Any initial condition $a(0)$ of this first-order equation will be attracted to a periodic orbit. The transient (and the resulting orbit) is described by an explicit solution

$$a = Q^{1/2}(\tau)\exp\left[-\mathrm{i}\frac{\operatorname{Im}\hat{\zeta}}{\hat{\alpha}}\int_0^\tau Q(\tau')\,\mathrm{d}\tau'\right], \tag{78}$$

where

$$Q(\tau) = \frac{Q_\infty}{1 - \mathrm{e}^{-\mu(\tau+\tau_0)}} \tag{79}$$

for large perturbations of the soliton: $|a(0)|^2 > Q_\infty \equiv \hat{\beta}\hat{h}/\operatorname{Re}\hat{\zeta}$, and

$$Q(\tau) = \frac{Q_\infty}{1 + \mathrm{e}^{-\mu(\tau-\tau_0)}} \tag{80}$$

for small initial conditions: $|a(0)|^2 < Q_\infty$. Here $\mu = 1/Q_\infty$, and τ_0 is an arbitrary positive constant.

Thus, unlike the weakly dissipative regime, no unbounded trajectories arise for $\gamma \sim 1$. In terms of the full, nonreduced NLS equation this means that in the strongly dissipative case, the unstable stationary soliton ψ_+ will necessarily evolve into a (stable) temporally periodic soliton $\psi_\sim$. Although the finite-dimensional periodic orbit is stable with respect to arbitrarily large perturbations, this does not guarantee, of course, that the soliton $\psi_\sim$ will be stable against arbitrarily large perturbations within the full NLS equation. We also need to emphasize here that the amplitude equation (37) is only valid in the vicinity of the Hopf bifurcation. Numerical simulations showed that for driving strengths further away from $\mathfrak{h} = \mathfrak{h}_c(\gamma)$, the oscillating soliton loses its stability to a double-periodic or chaotic attractor [4]. These higher bifurcations are not captured by the present asymptotic approach.

5. Long-term evolution of the oscillatory instability

5.1. Numerical simulations

In the case of finite γ, conclusions of our finite-dimensional analysis are in agreement with earlier computer simulations [4] where the unstable stationary soliton ψ_+ was seen to evolve into a temporally periodic soliton $\psi_\sim$. In the undamped case, on the contrary, our analysis shows that the oscillatory instability should result in a more fundamental transformation of the soliton. This case was not studied numerically before whereas the reduced amplitude equation provides no clue to what the corresponding asymptotic attractors should be. The case of *small* γ is intermediate; here the instability can give rise both to the oscillating soliton and to some other, yet unknown, attractors. With the aim of gaining some insight into the nature of these attractors as well as verifying conclusions of our finite-dimensional analysis, we have performed a series of computer simulations of the full, nonreduced nonlinear Schrödinger equation (1).

We restricted ourselves to the undamped case, $\gamma = 0$. Our numerical scheme is a generalization of the split-step pseudospectral method [21] and was previously utilized in [4]. The method imposes periodic boundary conditions $\psi(L) = \psi(-L), \quad \psi_X(L) = \psi_X(-L)$, where the length of the spatial interval was chosen to be $2L = 152$. In order to emulate the infinite-line situation, a 'sound-absorbing' term $-\mathrm{i}\gamma(X)\psi$ is added on the right-hand side of equation (1). Here the function $\gamma(X)$ is almost zero within the subinterval $(-60, 60)$ and increases to the value of approximately 0.55 as $X \to \pm 76$:

$$\gamma(X) = 0.3\left[\tanh\left(\frac{X-70}{5}\right) - \tanh\left(\frac{X+70}{5}\right) + 2\right].$$

The effect of this term is to damp small-amplitude radiation waves emanating from the soliton and prevent their re-entry back into the system via the periodic boundaries. Typically we used $N = 2^{11} = 2048$ Fourier modes which implied the spatial resolution $\Delta X = 2L/N \approx 7.4 \times 10^{-2}$. Our time increment, $\Delta T = 1.0 \times 10^{-3}$, was chosen so that the stability condition [21] of this numerical scheme be in place: $\Delta T < (\Delta X)^2/\pi = 1.8 \times 10^{-3}$.

We set up the initial condition in the form (11), (12), (15):

$$\psi(X, 0) = A[U(AX) + \mathrm{i}V(AX)], \tag{81a}$$

with

$$U(x) = \operatorname{sech}(x) + 2\epsilon \operatorname{Re} a u_c(x) + \epsilon^2\{|a|^2 u_0(x) - 2 \operatorname{Im} \dot{a} u_1(x) + 2 \operatorname{Re}[a^2 u_2(x)]\}, \tag{81b}$$

$$V(x) = -2\epsilon \operatorname{Im} a v_c(x) - 2\epsilon^2\{\operatorname{Re} \dot{a} v_1(x) + \operatorname{Im}[a^2 v_2(x)]\}. \tag{81c}$$

Here $a, \dot{a} =$ constant; u_c, v_c are the eigenfunctions of the operator (9) corresponding to $H = H_c$ and u_0, u_1, v_1, u_2, v_2 are solutions of the nonhomogeneous equations (16), (17), (19). The link to the reduced amplitude equation (28) is provided by setting the two constants, a and $\dot{a}$, equal to the initial values ($a(0)$ and $\dot{a}(0)$, respectively) of equation (28). Finally, A is given by equation (2*c*): $A = (1 + \mathfrak{h})^{1/2}$. Our choice of $\mathfrak{h}$ is related to the value of h used in simulations of the reduced system (28) in section 4.4 ($h = 0.1$). Taking $\epsilon = 0.1$, equation (14) gives $\mathfrak{h} = 0.064\,72$. (To get an idea of how close to the bifurcation point we are, recall that the oscillatory instability sets in at $\mathfrak{h}_c = 0.063\,59$.)

For all examined values of a and $\dot{a}$—provided $|E_3|$ (equation (49)) is not very large—the evolution starts with a relatively long period of growth of the oscillatory instability. During this transient period the field configuration may be regarded as a ψ_+ soliton with the amplitude and width oscillating about their stationary values (figure 6). After the amplitude of the growing perturbation has reached a certain critical value, a cross-over occurs and the subsequent evolution settles to one of the two possible asymptotic regimes. Both of these two attractors are localized in space and oscillate in time. In contrast to the transient phase, these oscillations are not about the stationary soliton but about $\psi = 0$ (see figures 6(*c*) and (*d*)). In both cases the oscillations of the soliton are accompanied by intensive radiation.

5.2. Asymptotic attractors

The first emerging attractor has a *negative* oscillation frequency with the magnitude slightly smaller than 1; it is bell-shaped and its amplitude is very slowly decaying in time (figure 6(*a*)). We will be referring to this solution as the *breather*; it is indeed a relative of the breather solution of the Klein–Gordon equation [22]. (Another, and possibly even closer relative is the soliton of the unperturbed NLS equation with the constant frequency shift, equation (1) with $\gamma = \mathfrak{h} = 0$.) Similarly to the Klein–Gordon breather, our breather lives in the gap of the continuous spectrum and can be constructed perturbatively.

To this end, we again decompose equation (1) with $\gamma = 0$ into its real and imaginary part and expand ψ in powers of a small parameter, ε:

$$\psi = U + \mathrm{i}V, \qquad U = \varepsilon(U_0 + \varepsilon^2 U_2 + \cdots), \qquad V = \varepsilon(V_0 + \varepsilon^2 V_2 + \cdots). \tag{82}$$

Here U_i and V_i depend on multiple space and time scales: $U_i = U_i(X, T; X_1, T_1)$, $V_i = V_i(X, T; X_1, T_1)$, where $X_1 = \varepsilon X$ and $T_1 = \varepsilon T$. The breather is therefore constructed as a perturbation of the trivial solution $\psi = 0$ with a small (but finite) amplitude. At the first order in ε we have a linear equation

$$M \begin{pmatrix} U_0 \\ V_0 \end{pmatrix} \equiv \begin{pmatrix} -\partial^2/\partial X^2 + 1 + \mathfrak{h} & \partial/\partial T \\ -\partial/\partial T & -\partial^2/\partial X^2 + 1 - \mathfrak{h} \end{pmatrix} \begin{pmatrix} U_0 \\ V_0 \end{pmatrix} = 0, \tag{83}$$

whose solutions are linear waves with the dispersion law $\omega^2 = 1 - \mathfrak{h}^2 + k^2$. Since we are primarily interested in nonpropagating structures, we take

$$\begin{pmatrix} U_0 \\ V_0 \end{pmatrix} = \varphi(X_1, T_2) \begin{pmatrix} 1 \\ i\xi \end{pmatrix} \mathrm{e}^{\mathrm{i}\omega T} + \text{c.c.}, \tag{84a}$$

where

$$\omega = \sqrt{1 - \mathfrak{h}^2} > 0, \qquad \xi = \frac{1 + \mathfrak{h}}{\omega} = \left(\frac{1 + \mathfrak{h}}{1 - \mathfrak{h}}\right)^{1/2}. \tag{84b}$$

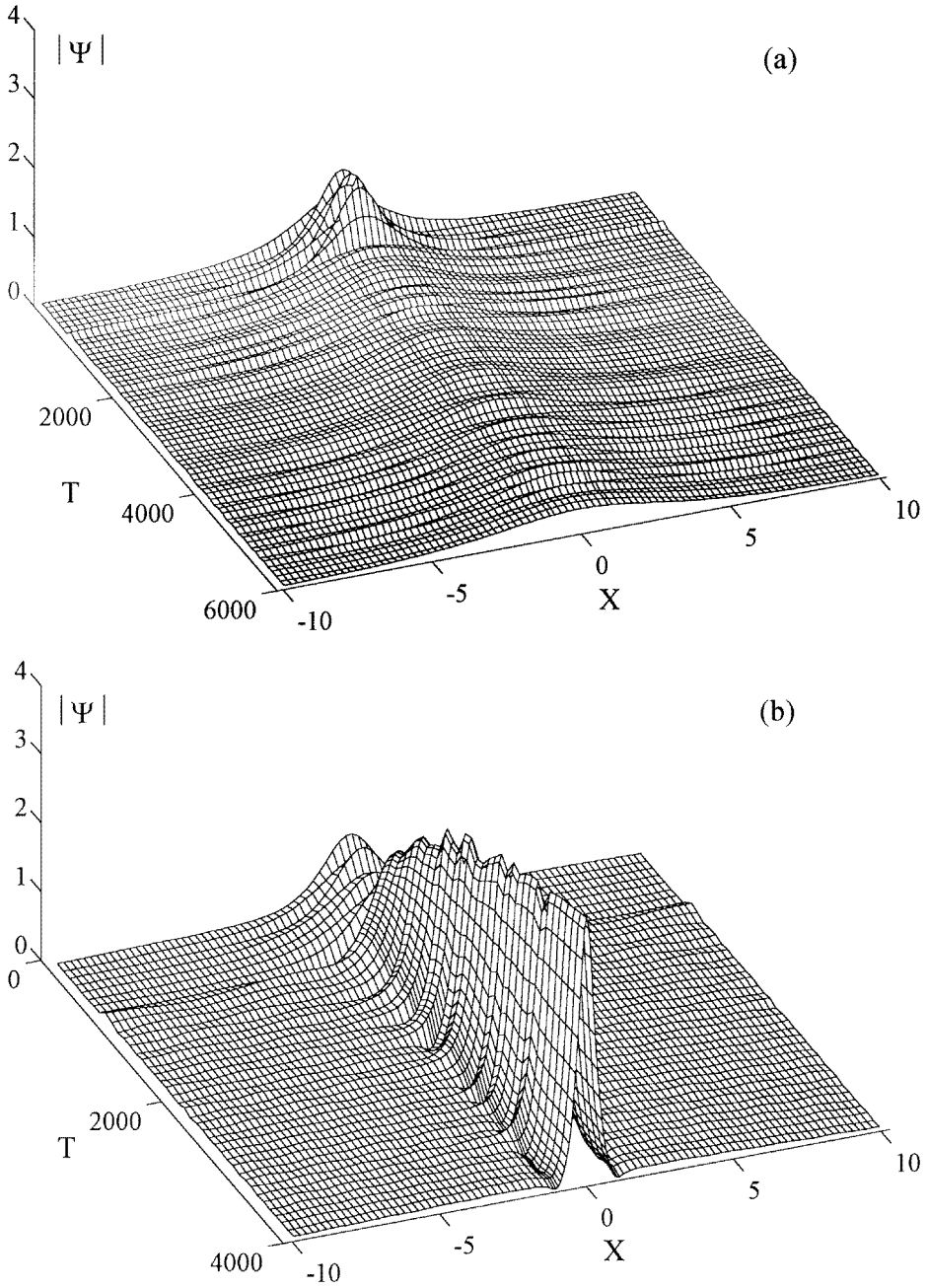

Figure 6. Evolution of the undamped soliton ($\gamma = 0$) perturbed by a perturbation of the form (81) with $|E_3| \sim 1$ (i.e. with $l(0) \sim 1$). For (*a*), (*c*): $a = -1$, $\dot{a} = \mathrm{i}$ and for (*b*), (*d*): $a = 1$, $\dot{a} = -\mathrm{i}$; in both cases $l(0) = -1$. All four pictures are obtained by means of numerical simulations of the full, nonreduced NLS equation (1). The simulations were carried out on an interval $[-76, 76]$; on (*a*), (*b*) the interval has been cut down for graphical clarity. On (*c*) and (*d*) plotted is the trajectory of the point $\psi(X = 0, T)$. The broken lines sketch the boundaries of basins of attraction of (*c*) $\psi_{\downarrow}$ and (*d*) $\psi_{\uparrow}$ attractor. The arrows indicate the direction of the evolution.

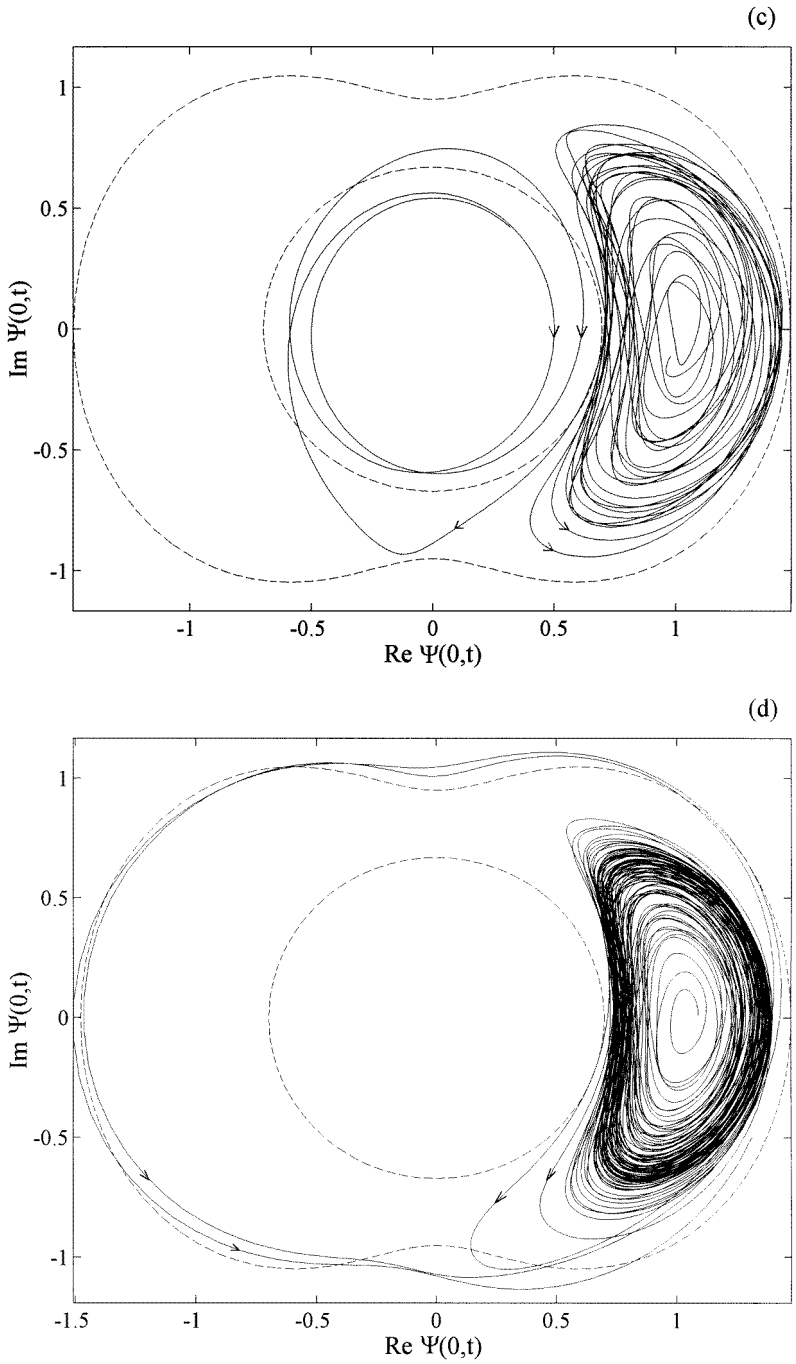

Figure 6. (Continued)

Next, at the order ε^2 we obtain

$$M\begin{pmatrix} U_2 \\ V_2 \end{pmatrix} = \begin{pmatrix} -\partial V_0/\partial T_2 + \partial^2 U_0/\partial X_1^2 + 2(U_0^2 + V_0^2)U_0 \\ \partial U_0/\partial T_2 + \partial^2 V_0/\partial X_1^2 + 2(U_0^2 + V_0^2)V_0 \end{pmatrix}. \tag{85}$$

Equation (85) is only solvable if the right-hand side is orthogonal (in the sense of the $\mathfrak{R}_2$-scalar product) to the vector $(1, -\mathrm{i}\xi)$. This gives the (undriven) NLS equation for φ:

$$-2\mathrm{i}\xi\frac{\partial\varphi}{\partial T_2} + (1+\xi^2)\frac{\partial^2\varphi}{\partial X_1^2} + 2(3+2\xi^2+3\xi^4)|\varphi|^2\varphi = 0, \tag{86}$$

with an obvious soliton solution. Returning to the original variable ψ, we can write our breather solution as

$$\psi_\downarrow = \varepsilon b\left(\frac{2(1-\mathfrak{h})}{2+\mathfrak{h}^2}\right)^{1/2}\left\{\frac{1+\xi}{2}\mathrm{e}^{-\mathrm{i}(\omega-\varepsilon^2b^2/\omega)T} + \frac{1-\xi}{2}\mathrm{e}^{\mathrm{i}(\omega-\varepsilon^2b^2/\omega)T}\right\} \times \operatorname{sech}(\varepsilon bX) + \mathrm{O}(\varepsilon^3), \tag{87}$$

where ω and ξ are given by equation (84*b*), and the amplitude $b = \mathrm{O}(1)$ is a slowly changing parameter, which is not defined at this order of the expansion. Note that for small $\mathfrak{h}$, ξ is close to 1 and the second term in (87) is negligible comparing to the first one. It is for this reason that in our numerical simulations the breather appears as a *negative* frequency solution. When $\mathfrak{h} = 0$, we have $\omega = 1$ and equation (87) is simply the soliton of the unperturbed NLS equation with the unit frequency shift.

The second localized attractor has *positive* oscillation frequency. Like the decaying soliton $\psi_\downarrow$, it is bell-shaped but its amplitude is growing with time (figure 6(*b*)). This large-amplitude soliton can also be constructed as a series in small parameter ε; this time we write

$$\psi = \varepsilon^{-1}(\psi_0 + \varepsilon^2\psi_2 + \cdots), \tag{88}$$

where the coefficients of the expansion depend on multiple scales: $\psi_i = \psi_i(X_{-1}, T_{-2}; X, T)$. Here $X_{-1} = \varepsilon^{-1}X$ and $T_{-2} = \varepsilon^{-2}T$. Substituting (88) into (1), the order ε^{-3} yields the unperturbed NLS equation:

$$\mathrm{i}\frac{\partial\psi_0}{\partial T_{-2}} + \frac{\partial^2\psi_0}{\partial X_{-1}^2} + 2|\psi_0|^2\psi_0 = 0 \tag{89}$$

and so the large-amplitude soliton is given by

$$\psi_\uparrow(X,T) = \frac{B}{\varepsilon}\exp\left(\mathrm{i}\frac{B^2}{\varepsilon^2}T\right)\operatorname{sech}\left(\frac{B}{\varepsilon}X\right) + \mathrm{O}(\varepsilon), \tag{90}$$

where $B = \mathrm{O}(1)$ is a slowly changing function of X and T which is not defined at this level of approximation.

Finding the exact laws of variation of b and B is beyond the scope of this work. We will restrict ourselves to commenting only on *why* the amplitude of the breather $\psi_\downarrow$ has to decay and the amplitude of the soliton $\psi_\uparrow$ to increase. As we mentioned in section 4, in the undamped case the equation (1) conserves energy,

$$E = \int\left[|\psi_X|^2 + |\psi|^2 - |\psi|^4 + \frac{\mathfrak{h}}{2}(\psi^2 + \psi^{*2})\right]\mathrm{d}X. \tag{91}$$

Substituting (87) into (91) yields the energy of the breather:

$$E_\downarrow = E[\psi_\downarrow] = \frac{4(1-\mathfrak{h}^2)}{2+\mathfrak{h}^2}\varepsilon b + \mathrm{O}(\varepsilon^3), \tag{92}$$

while doing the same with equation (90) gives the energy of the large-amplitude soliton:

$$E_\uparrow = E[\psi_\uparrow] \approx -\frac{2}{3}\left(\frac{B}{\varepsilon}\right)^3. \tag{93}$$

Since the linear radiation waves take away positive energy, the energies $E_\downarrow$ and $E_\uparrow$ have to decay. According to equation (92), this means that the amplitude b of the small-amplitude breather has to decrease. On the contrary, equation (93) implies that the amplitude of the large-amplitude soliton, B, will have to grow.

Thus, from the energy point of view, the difference between the two attractors $\psi_\downarrow$ and $\psi_\uparrow$ is that in the former case the energy of the breather decreases to zero (remaining positive all the time) whereas in the latter case the energy of the soliton is negative and tends to minus infinity.

A natural question is whether the type of the asymptotic regime (decay or growth) can be predicted from the analysis of the finite-dimensional dynamics described by equation (28) with a and $\dot{a}$ featuring in equation (81) taken as the initial values. Surprisingly, the answer is *no*. The evolutions shown in figures 6(*a*), (*c*) and (*b*), (*d*) correspond to the choices ($a = -1$, $\dot{a} = \mathrm{i}$) and ($a = 1$, $\dot{a} = -\mathrm{i}$), respectively. Although these initial conditions evolve into two completely different asymptotic regimes, the corresponding trajectories of the fictitious particle on the plane are identical up to a constant angular shift. In both cases the initial conditions of the particle are $r(0) = 1$, $\dot{r}(0) = 0$ and $l(0) = -1$; the corresponding trajectory is shown in figure 4(*b*).

The finite-dimensional system (28) is invariant with respect to constant phase shifts $a \to a\mathrm{e}^{\mathrm{i}\theta_0}$ while it is exactly the initial phase of the perturbation that plays the crucial role in the selection of one or the other asymptotic regime. This is shown symbolically in figures 6(*c*) and (*d*). The two broken closed contours demarcate what can roughly be considered as the boundaries of the basins of attraction of the decaying and growing soliton. Depending on the phase of $a(0)$ (i.e. depending on the initial angular position of the fictituous particle), the spiralling-out trajectory crosses the inner contour (schematically shown as a circle) or the outer one (a dumb-bell). In the first case the trajectory will remain within the inner contour, with the orbits of revolution slowly shrinking to the origin†. The corresponding solution of the NLS equation is attracted to the slowly decaying breather, $\psi_\downarrow$. In the second case the trajectory stays outside the dumb-bell, with the orbits slowly expanding. The corresponding NLS solution locks on to the growing soliton (90).

5.3. Large-energy initial conditions; evolution of the soliton ψ_-

The attractors $\psi_\downarrow$ and $\psi_\uparrow$ emerge if the energy $|E_3|$ of the perturbation is not very large (that is, if the initial position and velocity of the fictitious particle are of order 1). We have also studied the evolution of the initial condition corresponding to *large* $|E_3|$. (More specifically, we took $|\dot{a}(0)| \gg 1$ but $|a(0)| = \mathrm{O}(1)$.) As we remember from the simulations of the finite-dimensional system (28), the growth of $|a|^2$ is much faster in this case. Consistently with the finite-dimensional description, the transient in the evolution of the NLS soliton was indeed seen to be much shorter.

† These inner and outer contours should not be confused with the inner and outer circular bounds of the trajectory of the effective particle discussed in section 4.4. The equation of the fictitious particle describes growing oscillations of the field $\psi(X, T)$ about the unstable stationary soliton ψ_+ (i.e. about the point $\psi(0, T) = A$ in figures 6(*c*) and (*d*).) In contrast, the boundaries of the basins of attraction of the solitons $\psi_\downarrow$ and $\psi_\uparrow$ are centred at the origin. Furthermore, the effective-particle description is valid only while the amplitude of the oscillations is still small; it ceases to be applicable *before* the spiral crosses one of the broken closed contours in figures 6(*c*) and (*d*).

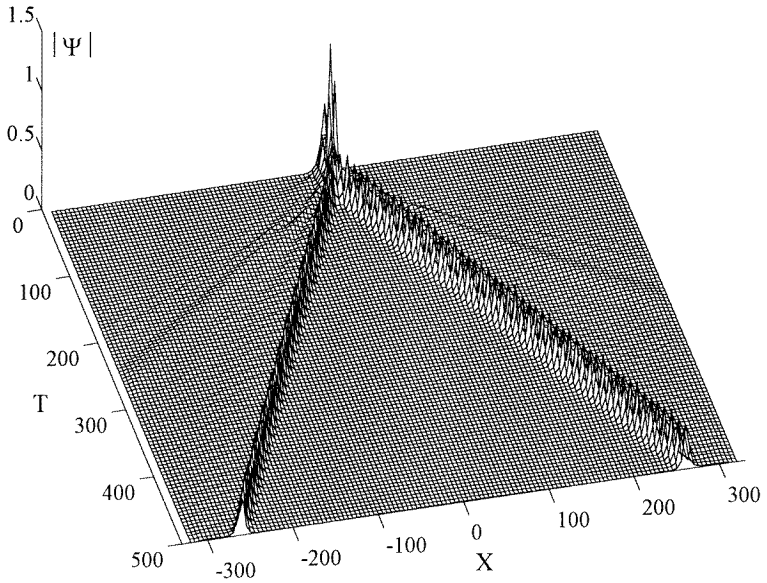

Figure 7. Evolution of the undamped soliton ($\gamma = 0$) perturbed by a perturbation of the form (81) with *large* negative E_3 (large negative l). Here $a = 1$, $\dot{a} = -18\mathrm{i}$ (and so $l(0) = -18$). The ψ_+ soliton splits into a couple of small-amplitude breathers $\psi_\downarrow$ equation (87), propagating in opposite directions and slowly decaying in time.

A more significant distinction arises at a later stage, when the unstable soliton splits into a pair of long-lived small-amplitude breathers $\psi_\downarrow$ travelling with constant velocities in opposite directions (figure 7). The explanation for this phenomenon is suggested by the spatial structure of the perturbation in this case, equation (81). A large initial value of $\dot{a}$ gives rise to a large $\{u_1, v_1\}$-component in the perturbation while both $u_1(x)$ and $v_1(x)$ have a sharp dip in the middle which serves as a nucleus of the future splitting.

Finally, we have simulated the evolution of the soliton ψ_- (equation (2)) which has a *positive* eigenvalue λ in its spectrum of linear excitations (and so is unstable with respect to a *nonoscillatory* mode). The initial condition was taken in the form

$$\psi(X, 0) = -\mathrm{i}A\,\mathrm{sech}(AX) - \mathrm{i}\epsilon A[u(AX) - v(AX)],$$

where this time A stands for $A_- = (1 - \mathfrak{h})^{1/2}$, and $\{u(x), v(x)\}$ is the eigenvector‡ of the operator (9) associated with the pure imaginary eigenvalue $\omega = -\mathrm{i}\lambda$. The subsequent evolution takes the soliton ψ_- to one of the two attractors observed in our simulations of the ψ_+ soliton. Namely, choosing $\epsilon < 0$ results in the slowly decaying breather (87) while in the $\epsilon > 0$ case one observes a slowly growing soliton (90). Thus, in the undamped case both the oscillatory and the translational, nonoscillatory, instability give rise to the same asymptotic attractors. The peculiarity of the oscillatory instability manifests itself only in the $\gamma \neq 0$ case, where it brings about a stably oscillating soliton.

‡ In the case of the ψ_- soliton the linearized operator has the same form as in the ψ_+ case, equations (7)–(9), where one only needs to replace $H \to -H$ and remember that now $H = -\mathfrak{h}/(1 - \mathfrak{h})$.

6. Concluding remarks and open problems

In this paper we have derived a reduced amplitude equation for the soliton in the vicinity of the oscillatory instability bifurcation. Bifurcations of this type occur in conservative and *weakly* dissipative wave systems. Similarly to the case of the Hopf instability (characteristic of *strongly* dissipative systems), the oscillatory instability sets in when a pair of complex-conjugate linearized eigenvalues crosses the imaginary axis. What makes the oscillatory instability bifurcation fundamentally different from the Hopf bifurcation, however, is the phenomenon of fusion and subsequent dissociation of a pair of stable eigenvalues which takes place just before the eigenvalues have acquired a positive real part. The oscillatory instability may therefore be regarded as a product of the resonance of two internal oscillation modes. As a consequence of the proximity to such resonance, the amplitude equation associated with the oscillatory instability is qualitatively different from the normal form of the Hopf bifurcation. (The former is second-order whereas the latter is a first-order equation.)

The second-order amplitude equation for the unstable perturbation admits a useful mechanical interpretation as an equation of planar motion of a classical particle in a radially-symmetric potential. The particle is also subject to a constant friction and time-independent torque which is induced by radiation waves emitted by the soliton. Exploiting this analogy and the associated classical mechanical formalism, we have demonstrated that in the $\gamma = 0$ case the presence of the torque always makes the trajectory of the fictitious particle unbounded. (The motion starts with quasiperiodic oscillations in an adiabatically changing ring which subsequently transform into a self-similar trajectory rapidly spiralling out.) In terms of the full nonreduced NLS dynamics, this means that the emission of radiation suppresses stably oscillating solitons. The finite-dimensional analysis provides no answer to *what* will be the resulting asymptotic attractors in this case, however.

In the *weakly* dissipative case (γ small but nonzero) the unbounded motions coexist with stable periodic orbits and therefore, the unstable stationary soliton may transform into a new soliton-like attractor which is localized in space and oscillates in time. Finally, in the *strongly* damped case ($\gamma \sim 1$), where the soliton's perturbations satisfy the complex Landau equation, unbounded finite-dimensional trajectories do not arise at all. Any perturbation of the unstable stationary soliton will necessarily have to evolve into a temporally periodic solitonic attractor.

In the undamped situation ($\gamma = 0$) the conclusions of the reduced finite-dimensional analysis have been verified in direct numerical simulations of the full, nonreduced NLS equation (1). In agreement with the effective particle description, no stably oscillating solitons were seen to arise. Our second aim here was to understand what are the infinite-dimensional counterparts of the unbounded finite-dimensional solutions; in other words, what localized or extended NLS attractors are represented by these spiralling-out trajectories. Depending on the initial perturbation, the decay of the unstable stationary soliton was observed to result in one of the two basic products: (a) a slowly decaying breather $\psi_{\downarrow}$, and (b) the soliton $\psi_{\uparrow}$ whose amplitude is increasing, slowly but indefinitely. Initial conditions with larger energy contents can give rise to a *pair* of small-amplitude breathers moving away from each other.

In the damped case ($\gamma \neq 0$) the numerical simulations of the NLS equation (1) were reported in [4]. Consistently, with our present conclusions, it was shown there that in some finite neighbourhood $\mathfrak{h} > \mathfrak{h}_c$ of the bifurcation value $\mathfrak{h}_c(\gamma)$ the unstable stationary soliton ψ_+ is replaced by a stable temporally-periodic soliton $\psi_{\sim}$. Here it is important to emphasize the difference between this soliton and what we refer to as the breather ($\psi_{\downarrow}$). Firstly, the soliton $\psi_{\sim}$ oscillates about the stationary soliton ψ_+, with the amplitude of oscillations being close to zero for $\mathfrak{h}$ close to $\mathfrak{h}_c$. On the contrary, the breather $\psi_{\downarrow}$ oscillates about the trivial solution $\psi = 0$, with the amplitude of oscillations being about one half of the amplitude of the

soliton ψ_+. Secondly, the frequency of the $\psi_\sim$ soliton is positive whereas the frequency of the breather $\psi_\downarrow$ is negative. Lastly and most importantly, the $\psi_\sim$ soliton does not decay whereas the breather has a long but finite lifetime.

Since the unbounded trajectories persist if a small damping is added, the small-amplitude breathers (and large-amplitude slowly growing solitons) should persist for small nonzero γ. However, adding even a small damping should drastically reduce the breather's lifetime. In this case the breather should arise only as a transient structure; the corresponding $T \to \infty$ asymptotic state will be trivial: $\psi = 0$. The trivial attractor was indeed observed in numerical simulations of [4]. It is appropriate to mention here that in [4] the unstable stationary soliton was perturbed only by the discretization errrors, i.e. the perturbation was always very weak. Speaking in the language of the fictitious particle, its initial radial position and velocity were always very small: $|a(0)|, |\dot{a}(0)| \sim 0$. The trajectory evolving from these initial conditions will necessarily be attracted to the stable periodic orbit. This explains the existence of a neighbourhood of the bifurcation value $\mathfrak{h}_c$ where the evolution of the unstable stationary soliton ψ_+ necessarily results in the periodic solution $\psi_\sim$ [4]. The trivial attractor $\psi = 0$ also exists in this neighbourhood but since the above-mentioned initial conditions lie ouside its basin of attraction, it did not arise in the numerical simulations of [4]. The trivial attractor was only observed for those $\mathfrak{h}$ where the periodic soliton $\psi_\sim$ becomes unstable, along with its double- and higher-periodic descendants.

It would be interesting to find out what is the $\gamma \neq 0$-counterpart of the growing soliton $\psi_\uparrow$. Computer simulations of the damped NLS equation (1) with $0.01 \leqslant \gamma \leqslant 0.02$ did exhibit a similar object which was seen to perform irregular walks, back and forth, over a strong radiation background [23]. This large-amplitude 'wandering' soliton was observed for fairly large values of $\mathfrak{h}$ ($\mathfrak{h} \approx 0.35$) whereas for $\mathfrak{h}$ in the immediate vicinity of $\mathfrak{h}_c(\gamma) \approx 0.07$ the decay of the unstable stationary soliton ψ_+ was seen to result in the stably oscillating soliton $\psi_\sim$. Interestingly, the 'wandering' soliton emerged for $\mathfrak{h}$ on the borderline between the region where the dominant attractor was trivial, $\psi = 0$, and the region where the unstable stationary soliton ψ_+ would 'ignite' a spatio-temporal chaotic state. A natural question is, therefore, on the relation between the large-amplitude soliton $\psi_\uparrow$ (slowly growing, oscillating and/or wandering) and spatio-temporal chaos. We are planning to return to this problem in future publications.

Finally, it is appropriate to mention a recent paper [24], whose author also uses singular perturbation expansions for the analysis of the parametrically driven NLS equation. However, the focus of [24] is on *stable* solitons and their response to *structural* perturbations (such as external fields, noise, etc) as well as soliton–soliton interactions. The present paper deals with completely different parameter range and completely different class of phenomena.

Acknowledgments

We are grateful to our colleagues Ben Herbst, Charles Hellaby, Norman Morrison, and Alan Rynhoud for discussions on various aspects of this work. Special thanks go to Professor Chris Brink for providing strong administrative and financial support. This project was also supported by research grants from FRD of South Africa and University Research Council of UCT.

Appendix

In this appendix we outline the scheme of numerical solution of the eigenvalue problem (9) and inhomogeneous equations (16)–(19). Some parts of this scheme are plain applications of

the Fourier method; other parts are not so straightforward yet general enough to be useful in the asymptotic analyses of other instances of radiating solitons.

A.1. Exponentially localized solutions

Expanding eigenfunctions u and v over cosines,

$$\begin{pmatrix} u(x) \\ v(x) \end{pmatrix} = \frac{1}{\sqrt{L}} \begin{pmatrix} u^{(0)} \\ v^{(0)} \end{pmatrix} + \sqrt{\frac{2}{L}} \sum_{n=1}^{\infty} \begin{pmatrix} u^{(n)} \\ v^{(n)} \end{pmatrix} \cos\left(\frac{\pi n x}{L}\right), \tag{94}$$

and truncating the series at $n = N$ reduces equation (9) to an eigenvalue problem for a block matrix:

$$\begin{pmatrix} \boldsymbol{\mathcal{L}}_1 & \mathbf{0} \\ \mathbf{0} & \boldsymbol{\mathcal{L}}_2 \end{pmatrix} \begin{pmatrix} \boldsymbol{u} \\ \boldsymbol{v} \end{pmatrix} = \omega \begin{pmatrix} \mathbf{0} & \boldsymbol{I} \\ \boldsymbol{I} & \mathbf{0} \end{pmatrix} \begin{pmatrix} \boldsymbol{u} \\ \boldsymbol{v} \end{pmatrix}. \tag{95}$$

Here $\boldsymbol{u}$ and $\boldsymbol{v}$ are $(N+1)$-dimensional column vectors: $\boldsymbol{u} = (u^{(0)}, u^{(1)}, \ldots, u^{(N)})^T$, $\boldsymbol{v} = (v^{(0)}, v^{(1)}, \ldots, v^{(N)})^T$ and $\boldsymbol{\mathcal{L}}_1$ and $\boldsymbol{\mathcal{L}}_2$ are $(N+1) \times (N+1)$ matrices with entries

$$\begin{aligned}
&\mathcal{L}_2^{(0,0)} = 1 - 2H - \frac{2}{L}, \qquad \mathcal{L}_1^{(0,0)} = 1 - \frac{6}{L}; \\
&\mathcal{L}_2^{(0,m)} = \mathcal{L}_2^{(m,0)} = -\frac{\sqrt{2}\pi^2 m}{L^2 \sinh\left(\frac{\pi^2 m}{2L}\right)}, \qquad \mathcal{L}_1^{(0,m)} = \mathcal{L}_1^{(m,0)} = 3\mathcal{L}_2^{(0,m)}; \\
&\mathcal{L}_2^{(m,n)} = \mathcal{L}_2^{(n,m)} = -\frac{\pi^2}{L^2}\left(\frac{m+n}{\sinh\left[\frac{\pi^2(m+n)}{2L}\right]} + \frac{m-n}{\sinh\left[\frac{\pi^2(m-n)}{2L}\right]}\right), \\
&\mathcal{L}_1^{(m,n)} = \mathcal{L}_1^{(n,m)} = 3\mathcal{L}_2^{(m,n)} \qquad (m, n = 1, \ldots, N, \quad m \neq n); \\
&\mathcal{L}_2^{(m,m)} = \left(\frac{\pi m}{L}\right)^2 + 1 - 2H - \frac{2}{L} - \frac{2\pi^2 m}{L^2 \sinh\left(\frac{\pi^2 m}{L}\right)}, \\
&\mathcal{L}_1^{(m,m)} = \left(\frac{\pi m}{L}\right)^2 + 1 - \frac{6}{L} - \frac{6\pi^2 m}{L^2 \sinh\left(\frac{\pi^2 m}{L}\right)}.
\end{aligned} \tag{96}$$

In equation (94) we restricted ourselves to the cosine series since u and v are assumed to be even. The matrices $\mathcal{L}_1$ and $\mathcal{L}_2$ are finite-dimensional approximations for the differential operators L_1 and L_2, respectively. In equation (96) we have also approximated finite-range integrals of the form $\int_0^L \operatorname{sech}^2(x) \cos\left(\frac{\pi m x}{L}\right) \mathrm{d}x$ by

$$\int_0^{\infty} \operatorname{sech}^2(x) \cos\left(\frac{\pi m x}{L}\right) \mathrm{d}x = \frac{\pi^2 m}{2L} \sinh\left(\frac{\pi^2 m}{2L}\right).$$

The introduced error is exponentially small in L. The normalization condition (13) for the eigenfunctions translates into the normalization condition for the Fourier coefficients:

$$2(\boldsymbol{u}^2 + \boldsymbol{v}^2) = 1. \tag{97}$$

The matrix eigenvalue problem (95)–(97) was solved by a standard numerical routine. Taking $L = 20$ with $N = 100$, 200 and 400, we have found $H_c = 0.059\,7928$, $\omega_c = 0.830\,28$ and $\beta = 1.644\,676$ in all cases, while increasing the interval twice ($L = 40$) gave $H_c = 0.059\,7933$, $\omega_c = 0.830\,294$ and $\beta = 1.644\,669$ (both for $N = 200$ and 400). Further increasing the interval ($L = 80$ with $N = 400$) did not bring any change to the last set of numbers.

The need for such a high accuracy stems from the fact that small errors in H_c, ω_c and hence the critical wavenumber (21), produce large errors in the asymptotic phase of the radiation-wave solution $u_2(x)$, $v_2(x)$ as $|x| \to \infty$. Since it is exactly the asymptotic phase that selects the particular solution we need (the outgoing wave), an inaccurately determined far-field phase would have resulted in an incorrect near-field behaviour of u_2, v_2 and eventually, in a highly inaccurate value of the integral ζ (equation (31)).

Having found the critical eigenvalue ω_c and the corresponding eigenvector $(\boldsymbol{u}_c, \boldsymbol{v}_c)$, we proceed to solution of the nonhomogeneous equation (17). Expanding

$$\begin{pmatrix} u_1(x) \\ v_1(x) \end{pmatrix} = \frac{1}{\sqrt{L}} \begin{pmatrix} u_1^{(0)} \\ v_1^{(0)} \end{pmatrix} + \sqrt{\frac{2}{L}} \sum_{n=1}^{\infty} \begin{pmatrix} u_1^{(n)} \\ v_1^{(n)} \end{pmatrix} \cos\left(\frac{\pi n x}{L}\right), \tag{98}$$

and substituting into (17) gives

$$\mathcal{M}_{\omega_c} \begin{pmatrix} \boldsymbol{u}_1 \\ \boldsymbol{v}_1 \end{pmatrix} \equiv \begin{pmatrix} \boldsymbol{\mathcal{L}}_1 & -\omega_c \boldsymbol{I} \\ -\omega_c \boldsymbol{I} & \boldsymbol{\mathcal{L}}_2 \end{pmatrix} \begin{pmatrix} \boldsymbol{u}_1 \\ \boldsymbol{v}_1 \end{pmatrix} = - \begin{pmatrix} \boldsymbol{v}_c \\ \boldsymbol{u}_c \end{pmatrix}, \tag{99}$$

with $\boldsymbol{u}_1 = (u_1^{(0)}, u_1^{(1)}, \ldots, u_1^{(N)})^T$ and $\boldsymbol{v}_1 = (v_1^{(0)}, v_1^{(1)}, \ldots, v_1^{(N)})^T$. Although the matrix $\mathcal{M}_{\omega_c}$ has a zero eigenvalue, the solvability of this linear system is guaranteed by the fact that the associated eigenvector $\{\boldsymbol{u}_c, \boldsymbol{v}_c\}$ satisfies the condition (22):

$$\boldsymbol{u}_c \cdot \boldsymbol{v}_c = 0. \tag{100}$$

In order to factor out the linear subspace spanned by this eigenvector, we decompose the singular matrix as $\mathcal{M}_{\omega_c} \mathcal{E} = \mathcal{Q}\mathcal{R}$, where $\mathcal{R}$ is upper-triangular and $\mathcal{Q}$ orthogonal matrix. Equation (99) is transformed to the upper triangular form:

$$\mathcal{R} \begin{pmatrix} \tilde{\boldsymbol{u}}_1 \\ \tilde{\boldsymbol{v}}_1 \end{pmatrix} = -\mathcal{Q}^T \begin{pmatrix} \boldsymbol{v}_c \\ \boldsymbol{u}_c \end{pmatrix}, \tag{101}$$

where

$$\begin{pmatrix} \tilde{\boldsymbol{u}}_1 \\ \tilde{\boldsymbol{v}}_1 \end{pmatrix} = \mathcal{E}^{-1} \begin{pmatrix} \boldsymbol{u}_1 \\ \boldsymbol{v}_1 \end{pmatrix} \tag{102}$$

and $\mathcal{E}$ is a permutation matrix which is chosen so that to make the zero diagonal element of the matrix $\mathcal{R}$ appear in the lower right corner. The matrix $\mathcal{Q}$ will then contain the vector $\{\boldsymbol{u}_c, \boldsymbol{v}_c\}$ as its last column and by virtue of equation (100), the last component of the vector on the right-hand side of equation (101) will be zero. Hence, in order to solve the linear system (101) it is sufficient to discard its last equation (which is simply $0 \cdot \tilde{v}_1^{(N+1)} = 0$). The resulting system of $(2N+1)$ equations has a nonsingular matrix and can be solved by a standard routine. After that we put $\tilde{v}_1^{(N+1)} = 0$ and use equation (102) to recover a solution of the original system (99). (Choosing any other value for $\tilde{v}_1^{(N+1)}$ amounts to adding $\tilde{v}_1^{(N+1)} \times \{u_c, v_c\}$ to the solution $\{u_1, v_1\}$; in view of the orthogonality relation (22) this does not affect the value of α, equation (29).)

The accuracy of the computation can be judged by the values of the integral (29). Choosing $L = 20$ with $N = 100$, 200 and 400 we obtained $\alpha = 1.330\,575$ in all cases; doubling the interval length with $N = 200$ and 400 gave $\alpha = 1.329\,676$; finally taking $L = 80$ with $N = 400$ produced $\alpha = 1.329\,675$.

The nonhomogeneous equation (16) is solved in a similar way. The only difference is that since the homogeneous solution of equation (16) is an odd function, the matrix $\boldsymbol{\mathcal{L}}_1$ is nonsingular and so there is no need in the diagonalization in this case.

A.2. Radiation waves: the two-interval technique

The solution of the boundary-value problem (19), (20) turns out to be somewhat more laborious. As we have already mentioned in section 2.2, equation (19) has a bounded homogeneous solution:

$$\begin{pmatrix} L_1 & -2\omega_c \\ -2\omega_c & L_2 \end{pmatrix} \begin{pmatrix} u_h \\ v_h \end{pmatrix} = 0. \tag{103}$$

This solution is the eigenfunction of the operator (9) associated with the continuous spectrum eigenvalue $\omega = 2\omega_c$. In general, the forcing term on the right-hand side of (19) will not satisfy the condition of solvability of equation (19) in the class of square-integrable functions:

$$\int_{-\infty}^{\infty} \{u_h, v_h\} \cdot \begin{pmatrix} 3u_c^2 - v_c^2 \\ 2u_c v_c \end{pmatrix} U_0 \, \mathrm{d}x = 0. \tag{104}$$

This does not mean, of course, that *nondecaying* nonhomogeneous solutions do not exist. Quite the contrary, from the fact that u_h, v_h undergo nondecaying oscillations as $|x| \to \infty$ one can readily deduce that the nonhomogeneous equation (19) has oscillatory solutions. We need to construct the solution $\{u_2, v_2\}$ satisfying the radiation conditions (20) at infinity; the problem, however, is that the Fourier method can only be implemented on *finite* intervals. This difficulty can be circumvented by making use of *two* finite intervals; our method is as follows.

First, we observe that the homogeneous equation (103) will not, in general, have solutions with periodic boundary conditions $u_h(L) = u_h(-L)$, $u_h'(L) = u_h'(-L)$ (and similarly for v_h). The periodic solutions will arise only for particular values of L. (Here we assume that L is large enough ($L \gg 1$) so that when $|x| \sim L$, the functions $u_h(x)$ and $v_h(x)$ will have settled to their oscillatory asymptotes.) For these *resonant* values of L and for sufficiently large $|x| \sim L$ we will have then

$$u_h \to A \cos\{k_c(|x| - L)\} \tag{105}$$

and a similar relation for v_h. Next, since the operator $M_{2\omega_c}$ has a zero eigenvalue with the associated eigenfunction periodic on the interval $(-L, L)$, the nonhomogeneous equation (19) does not have a periodic solution on this interval. We can, however, solve it on a nonresonant interval $(-\tilde{L}, \tilde{L})$, where $\tilde{L} \neq L$; we will denote the corresponding solution $\{\tilde{u}_2, \tilde{v}_2\}$. The functions on the right-hand side of equation (19) fall with distance as $\mathrm{e}^{-|x/x_0|}$, where $x_0 \approx 0.6$†; consequently we should choose $\tilde{L} \gg 1$. Then, for sufficiently large $|x| \sim \tilde{L}$ we have

$$\tilde{u}_2 \to B \cos\{k_c(|x| - \tilde{L})\} \tag{106}$$

and a similar relation for $\tilde{v}_2$.

Finally, the nonhomogeneous solution satisfying the radiation condition (20) can be constructed as a linear combination of the nonhomogeneous solution $\{\tilde{u}_2, \tilde{v}_2\}$, periodic with period $2\tilde{L}$, and the even homogeneous solution $\{u_h, v_h\}$ periodic with period $2L$:

$$\begin{pmatrix} u_2 \\ v_2 \end{pmatrix} = \begin{pmatrix} \tilde{u}_2 \\ \tilde{v}_2 \end{pmatrix} + C \begin{pmatrix} u_h \\ v_h \end{pmatrix}. \tag{107}$$

Substituting (105), (106) and (107) into (20) and setting the coefficients of $\exp\{\mathrm{i}k_c|x|\}$ to zero, we find the value of C:

$$C = -\frac{B}{A} \mathrm{e}^{\mathrm{i}k_c(L-\tilde{L})}, \tag{108}$$

† More precisely, $1/x_0 = 1 + 2\kappa_c$, where κ_c is the decay rate of $u_c(x)$ and $v_c(x)$: $\kappa_c^2 = 1 - H_c - \sqrt{H_c^2 + \omega_c^2}$.

while comparing coefficients of $\exp\{-ik_c|x|\}$ gives a simple relation between $\mathcal{R}$, the amplitude of the radiation at infinity, and B, the amplitude of the nonhomogeneous solution periodic on the interval $(-\tilde{L}, \tilde{L})$:

$$B = -i\mathcal{R}\frac{e^{-ik_cL}}{\sin\{k_c(\tilde{L}-L)\}}. \tag{109}$$

This formula is another manifestation of the fact that the inhomogeneous problem cannot be solved on the resonant interval $(-L, L)$ on which the homogeneous solution was found. The smaller is the difference $|\tilde{L}-L|$, the greater will be the amplitude B and, according to (108), the larger coefficient C we will have to take in equation (107) in order to offset the ingoing component of the radiation wave. Consequently, the less accurate will be the resulting solution $u_2(x)$.

From the above construction it is also clear why we did not invoke *odd* homogeneous solutions. Adding an odd homogeneous solution to the function $u_2(x)$ given by equation (107) with C fixed by equation (108), would bring an uncompensated ingoing wave $\sim e^{ik_c|x|}$ thereby violating the radiation condition. For this reason we have identified the amplitudes of the right and left outgoing waves in section 2.2: $\mathcal{R}^+ = \mathcal{R}^- \equiv \mathcal{R}$.

In order to implement the above procedure numerically, we expand

$$\begin{aligned}
&\begin{pmatrix} u_2(x) \\ v_2(x) \end{pmatrix} = \frac{1}{\sqrt{L}}\begin{pmatrix} u_2^{(0)} \\ v_2^{(0)} \end{pmatrix} + \sqrt{\frac{2}{L}}\sum_{n=1}^{\infty}\begin{pmatrix} u_2^{(n)} \\ v_2^{(n)} \end{pmatrix}\cos\left(\frac{\pi nx}{L}\right), \\
&2U_0(x)\begin{pmatrix} 3u_c^2(x) - v_c^2(x) \\ 2u_c(x)v_c(x) \end{pmatrix} = \frac{1}{\sqrt{L}}\begin{pmatrix} s_0 \\ t_0 \end{pmatrix} + \sqrt{\frac{2}{L}}\sum_{n=1}^{\infty}\begin{pmatrix} s_n \\ t_n \end{pmatrix}\cos\left(\frac{\pi nx}{L}\right).
\end{aligned} \tag{110}$$

Truncating the series at $n = N$, equation (19) is converted to a linear algebraic system

$$\mathcal{M}_{2\omega_c}\begin{pmatrix} \boldsymbol{u}_2 \\ \boldsymbol{v}_2 \end{pmatrix} \equiv \begin{pmatrix} \boldsymbol{\mathcal{L}}_1 & -2\omega_c \\ -2\omega_c & \boldsymbol{\mathcal{L}}_2 \end{pmatrix}\begin{pmatrix} \boldsymbol{u}_2 \\ \boldsymbol{v}_2 \end{pmatrix} = \begin{pmatrix} \boldsymbol{s} \\ \boldsymbol{t} \end{pmatrix}, \tag{111}$$

where $\boldsymbol{u}_2$, $\boldsymbol{v}_2$, $\boldsymbol{s}$ and $\boldsymbol{t}$ are $(N+1)$-dimensional vectors, e.g. $\boldsymbol{u}_2 = (u_2^{(0)}, u_2^{(1)}, \ldots, u_2^{(N)})^T$. For resonant interval lengths L the matrix $\mathcal{M}_{2\omega_c}$ will have zero among its $2(N+1)$ eigenvalues $\mu_0, \mu_1, \ldots, \mu_{2N+1}$. The resonant lengths can be found with any desirable accuracy. In particular, taking $L = 20.117\,25$ with 100 Fourier modes yields the smallest modulus eigenvalue $\mu_\alpha = 1.1\times10^{-6}$. The choices $L = 38.610\,176$ with $N = 200$ and $L = 79.295\,415$ with $N = 400$ result in $\mu_\alpha = 3.7\times10^{-7}$ and $\mu_\alpha = 3.6\times10^{-7}$, respectively. The associated eigenvectors give a reasonably accurate approximation for the even homogeneous solution (u_h, v_h) of equation (19), periodic with period $2L$.

Next, by varying intervals slightly, $L \to \tilde{L}$, we can always ensure that the smallest modulus eigenvalue $\tilde{\mu}_\alpha$ is not *very* small. In particular, choosing $\tilde{L} = 19.65$ with $N = 100$ gives $\tilde{\mu}_\alpha = 3.5\times10^{-2}$; for $\tilde{L} = 38$ with $N = 200$ and $\tilde{L} = 78.65$ with $N = 400$ one obtains $\tilde{\mu}_\alpha = 2.4\times10^{-2}$ and $\tilde{\mu}_\alpha = 1.2\times10^{-2}$, respectively. We solved the nonhomogeneous system (111) in each of these cases. The resulting even nonhomogeneous solution $\tilde{u}_2$, $\tilde{v}_2$ is, of course, periodic with period $2\tilde{L}$: $\tilde{u}_2'(0) = \tilde{u}_2'(\tilde{L}) = 0$; $\tilde{v}_2'(0) = \tilde{v}_2'(\tilde{L}) = 0$. These boundary conditions are imposed by making use of the Fourier expansions.

After $\tilde{L}$ has been picked up not very close to L, the dominant error in the numerically found solution u_2, v_2 comes from the *finiteness* of the interval $(-\tilde{L}, \tilde{L})$. The truncation of the infinite interval results in the δ-function peak in the Fourier transform of $\tilde{u}_2(x)$, $\tilde{v}_2(x)$ being replaced by the *sinc*-function:

$$\mathcal{R}\delta(k-k_c) \longrightarrow \mathcal{R}\frac{\tilde{L}}{\pi}\frac{\sin\{(k-k_c)\tilde{L}\}}{(k-k_c)\tilde{L}} \equiv \mathcal{R}\frac{\tilde{L}}{\pi}\,\mathrm{sinc}\{(k-k_c)\tilde{L}\}. \tag{112}$$

Table 1.

	$\mathrm{Re}\,\zeta$	$\mathrm{Im}\,\zeta$, equation (31)	$\mathrm{Im}\,\zeta$, equation (32)
$L = 79.295\,415$, $\tilde{L} = 79.0$, $N = 400$	8.42×10^{-2}	1.92×10^{-3}	2.55×10^{-3}
$L = 119.9807$, $\tilde{L} = 119.75$, $N = 600$	8.15×10^{-2}	1.84×10^{-3}	2.22×10^{-3}
$L = 179.159\,22$, $\tilde{L} = 178.95$, $N = 600$	7.95×10^{-2}	1.76×10^{-3}	2.00×10^{-3}

Next, k can only assume a discrete set of values: $k = k_n = \pi n/\tilde{L}$, where $n = 0, 1, \ldots, N$. In general, *two* values of k, say k_m and k_{m+1}, will fall into the central lobe of the *sinc*-function: $k_c - \pi/\tilde{L} < k_m < k_{m+1} < k_c + \pi/\tilde{L}$. Accordingly, the solution $\tilde{u}_2$, $\tilde{v}_2$ will approach a linear combination of *two* cosines, $\cos(k_m x)$ and $\cos(k_{m+1} x)$, as $x \to \infty$. On the top of that, additional wavenumber components will be introduced by the sidelobes of the *sinc*-function, and thus the asymptotic waveform may substantially deviate from $\cos(k_c x)$.

These undesirable numerical effects can be reduced by increasing the interval length. First, the width of the central lobe of the *sinc*-function is equal to $2\pi/\tilde{L}$; as $\tilde{L}$ is increased, the central lobe narrows and the error in the asymptotic wavenumber reduces as $1/\tilde{L}$. Second, the amplitude of the central lobe grows in proportion to $\tilde{L}$ whereas amplitudes of the sidelobes remain constant. Hence, increasing the interval length suppresses the leakage to the sidelobes as well.

With the solution of the boundary value problem (19), (20) at hand, we can evaluate the coefficient ζ, equation (31). The imaginary part of ζ can be recomputed in a different way: instead of doing the integral (31), we identify the amplitude B from the asymptotic behaviour of $\tilde{u}_2(x)$ (see equation (105)); then recover the amplitude $\mathcal{R}$ from equation (109) and finally, use equation (32). The discrepancy between the two answers for $\mathrm{Im}\,\zeta$ provides an estimate for the accuracy of the computation.

We have carried out three series of calculations for the increasing values of L, $\tilde{L}$ and N. Results are presented in table 1.

When plotted versus $1/L$, the values of $\mathrm{Re}\,\zeta$ lie on the same straight line. The linear extrapolation to $L = \infty$ gives $\mathrm{Re}\,\zeta = (7.5555 \pm 0.0005) \times 10^{-2}$. The corresponding values of the imaginary part of the integral (31) (second column in table 1) also change linearly with $1/L$. Extrapolating to infinity we get $\mathrm{Im}\,\zeta = (1.60 \pm 0.02) \times 10^{-3}$. On the other hand, the linear extrapolation of $\mathrm{Im}\,\zeta$ obtained by means of the far-field formula (32) gives $\mathrm{Im}\,\zeta = (1.59 \pm 0.04) \times 10^{-3}$ which agrees well with the result of the numerical integration.

References

[1] Juul Rasmussen J and Rypdal K 1986 *Phys. Scr.* **33** 481
Turitsyn S K 1992 *Singularities in Fluids, Plasmas and Optics (NATO ASI Series)* ed R Caflisch (Dordrecht: Kluwer Academic)

[2] Eilbeck J C, Lomdahl P S and Newell A C 1981 *Phys. Lett.* A **87** 1
Bishop A R, Fesser K, Lomdahl P S and Trullinger S E 1983 *Physica* D **7** 259
Overman E A, McLaughlin D W and Bishop A R 1986 *Physica* D **19** 1
Nozaki K and Bekki N 1983 *Phys. Rev. Lett.* **50** 1226
Nozaki K and Bekki N 1984 *Phys. Lett.* A **102** 383
Bishop A R, Forest M G, McLaughlin D W and Overman II E A 1986 *Physica* D **23** 293

[3] Umeki M 1991 *J. Phys. Soc. Japan* **60** 146
Umeki M 1991 *J. Fluid Mech.* **227** 161
Kambe J and Umeki M 1990 *J. Fluid Mech.* **212** 373

[4] Bondila M, Barashenkov I V and Bogdan M M 1995 *Physica* D **87** 314

[5] Barashenkov I V and Panova E Yu 1993 *Physica* D **69** 114

[6] Kuznetsov E A, Rubenchik A M and Zakharov V E 1986 *Phys. Rep.* **142** 103

[7] Pelinovsky D E and Grimshaw R H J 1997 *Nonlinear Instability Analysis (Advances in Fluid Mechanics)* ed L Debnath and S Choudhury (Southampton: Computational Mechanics Publications) ch 8
[8] Pelinovsky D E, Afanasjev V V and Kivshar Yu S 1996 *Phys. Rev.* E **53** 1940
Pelinovsky D E, Kivshar Yu S and Afanasjev V V 1998 *Physica* D **116** 121
[9] Pelinovsky D E, Kivshar Yu S and Afanasjev V V 1996 *Phys. Rev.* E **54** 2015
[10] Barashenkov I V, Zhanlav T and Bogdan M M 1990 *Nonlinear World: IY International Workshop on Nonlinear and Turbulent Processes in Physics (Kiev, 9–22 October 1989)* ed V G Bar'yakhtar *et al* (Singapore: World Scientific) p 3
Terrones G, McLaughlin D W, Overman E A and Pearlstein A J 1990 *SIAM J. Appl. Math.* **50** 791
Barashenkov I V and Smirnov Yu S 1996 *Phys. Rev.* E **54** 5707
[11] Barashenkov I V, Bogdan M M and Korobov V I 1991 *Europhys. Lett.* **15** 113
[12] Pego R L, Smereka P and Weinstein M I 1995 *Nonlinearity* **8** 921
[13] Wu J, Keolian R and Rudnick I 1984 *Phys. Rev. Lett.* **52** 1421
Laedke E W and Spatschek K H 1991 *J. Fluid. Mech.* **223** 589
Yan J R and Mei Y P 1993 *Europhys. Lett.* **23** 335
Chen X-N and Wei R-J 1994 *J. Fluid Mech.* **259** 291
Wang X and Wei R 1994 *Phys. Lett.* A **192** 1
Wang X and Wei R 1997 *Phys. Lett.* A **227** 55
Wang X and Wei R 1997 *Phys. Rev. Lett.* **78** 2744
[14] Miles J W 1984 *J. Fluid Mech.* **148** 451
[15] Zakharov V E, Musher S L and Rubenchik A M 1985 *Phys. Rep.* **129** 285
Yajima N and Tanaka M 1988 *Prog. Theor. Phys. Suppl.* **94** 138
[16] Zakharov V E, L'vov V S and Starobinets S S 1975 *Sov. Phys.–Usp.* **17** 896
L'vov V S *et al* 1973 *Fizika Tverdogo Tela* **15** 793
Yamazaki H and Mino M 1989 *Prog. Theor. Phys. Suppl.* **98** 400
[17] Bogdan M M, Kosevich A M and Manzhos I V 1985 *Sov. J. Low Temp. Phys.* **11** 547
[18] Deutsch I H and Abram I 1994 *J. Opt. Soc. Am.* B **11** 2303
Longhi S 1995 *Opt. Lett.* **20** 695
Mecozzi A, Kath L, Kumar P and Goedde C G 1994 *Opt. Lett.* **19** 2050
[19] Pagano S, Salerno M and Samuelsen M R 1987 *Physica* D **26** 396
Grønbech-Jensen N, Kivshar Y S and Samuelsen M R 1993 *Phys. Rev.* B **47** 5013
Grauer R and Kivshar Y S 1993 *Phys. Rev.* E **48** 4791
[20] Guckenheimer J and Holmes P 1983 *Nonlinear Oscillations, Dynamical Systems and Bifurcations of Vector Fields* (Berlin: Springer)
Marsden J and McCracken M 1976 *The Hopf Bifurcation and Its Applications* (Berlin: Springer)
[21] Weideman J A C and Herbst B M 1986 *SIAM J. Numer. Anal.* **23** 485
[22] Kosevitch A M and Kovalev A S 1974 *Zh. Eksper. Teoret. Fiz.* **67** 1793 (Engl. transl. 1974 *Sov. Phys.–JETP* **40** 891)
Dashen R F, Hasslacher B and Neveu A 1974 *Phys. Rev.* D **10** 4130
Segur H and Kruskal M D 1987 *Phys. Rev. Lett.* **58** 747
Boyd J P 1990 *Nonlinearity* **3** 177
[23] Bondila M 1995 *MSc Thesis* University of Cape Town, unpublished
[24] Longhi S 1997 *Phys. Rev.* E **55** 1060